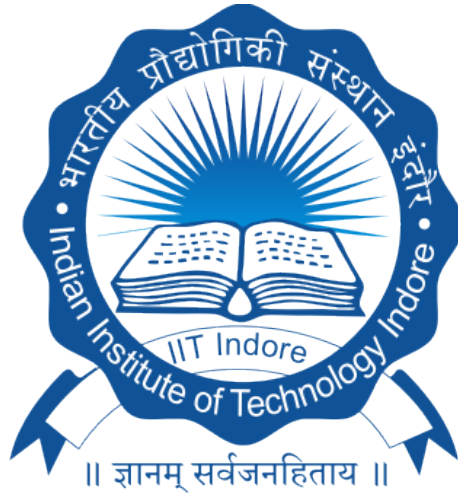


**TIFR-GMRT SKY SURVEY (TGSS):  
AN ALTERNATE APPROACH TO DATA  
ANALYSIS**

**M.Sc. Thesis**

**By:  
Pranoy Ghosh**



**DEPARTMENT OF ASTRONOMY , ASTROPHYSICS AND  
SPACE ENGINEERING**

**INDIAN INSTITUTE OF TECHNOLOGY  
INDORE**

**June, 2021**

**TIFR-GMRT SKY SURVEY (TGSS):  
AN ALTERNATE APPROACH TO DATA  
ANALYSIS**

**A THESIS**

*Submitted in partial fulfillment of the  
requirements for the award of the degree  
of  
Master of Science*

*by*  
**Pranoy Ghosh**



**DEPARTMENT OF ASTRONOMY , ASTROPHYSICS AND  
SPACE ENGINEERING**

**INDIAN INSTITUTE OF TECHNOLOGY  
INDORE**

**June, 2021**

**INDIAN INSTITUTE OF TECHNOLOGY INDORE**  
**CANDIDATE'S DECLARATION**

I hereby certify that the work which is being presented in the thesis entitled “**TIFR-GMRT SKY SURVEY (TGSS): AN ALTERNATE APPROACH TO DATA ANALYSIS**” in the partial fulfillment of the requirements for the award of the degree of MASTER OF SCIENCE and submitted in the Department of Astronomy, Astrophysics and Space Engineering, Indian Institute of Technology Indore, is an authentic record of my own work carried out during the time period from July, 2020 to May, 2021 under the supervision of Dr. Abhirup Datta (Associate Professor, IIT Indore) and Dr. C.H. Ishwara Chandra (Associate Professor, NCRA-TIFR). The matter presented in this thesis has not been submitted by me for the award of any other degree of this or any other institute.

*Pranoy Ghosh*  
10/06/2021

**Signature with date  
(Pranoy Ghosh)**

---

This is to certify that the above statement made by the candidate is correct to the best of my knowledge.

*Abhirup Datta*

10/06/2021

Signature of the Supervisor 1  
**(Dr. Abhirup Datta)**

*Ishwara Chandra*  
10/6/21

Signature of the Supervisor 2  
**(Dr. C.H. Ishwara Chandra)**

---

**Pranoy Ghosh** has successfully given his M.Sc. Oral Examination held on .....*9/06/2021*.....  
(*9<sup>th</sup> June 2021*)



Signature(s) of the Supervisor(s)  
of M.Sc. Thesis, Date: 10/06/2021

Suman Majumdar  
10/06/2021

Signature of Convener,  
DPGC, Date:



Signature of M.Sc. coordinator  
DAASE  
Date:- 10-06-2021



Signature of Head of Department  
DAASE  
Date:- 10/06/2021



Signature of  
PSPC Member 1  
Date:-  
Dr. A. K. Singh, 11/06/2021



Signature of  
PSPC Member 2  
Date:-10-06-2021



10/06/2021  
Signature of  
PSPC Member 3  
Date:-

## ACKNOWLEDGEMENT

If words are considerable as symbols of approval and taken as acknowledgment then let the words play a leading role in expressing my gratitude to my parents Shri. Pranab Kumar Ghosh and Smt. Sikha Ghosh for they do all household works to spare time for my research.

I also take the opportunity to express my sincere gratitude to both my supervisors- Dr. Abhirup Datta, Associate Professor, DAASE, IIT INDORE and Dr. Ishwara Chandra C.H., Associate Professor, NCRA-TIFR for their speedy and apt responses to my queries. Based on this work a talk titled ‘Reanalysis of TGSS: Better constraints on low frequency foregrounds’ was given in the recent EOR21 cosmology workshop April 19 - 23, 2021 (organized by SKA India CD/EoR Cosmology Science Working Group in support with NCRA-TIFR) and I must acknowledge the discussions that followed to be vital for the work in its current form. Finally I would like to acknowledge God’s grace and Prof. Yashwant Gupta, Director of NCRA-TIFR for his kind attention to arrange this golden opportunity for me through NCRA Student Program. Further since the project work is based on data which came from GMRT , we thank the staff of GMRT for making this observation possible. GMRT is run by National Centre for Radio Astrophysics of the Tata Institute of Fundamental Research.

I feel special thanks must go to my seniors namely-Aishrilla di, Arnab da, Akriti di, Swarna di and others (PhD Research Scholars in the Dr. Datta’s research group) whose valuable feedback and discussions I often looked forward to, and without them this work may not be in its current form.

Thankfully,  
Pranoy Ghosh

# ABSTRACT

“TIFR GMRT SKY SURVEY (TGSS)” is a continuum survey at 150 MHz conducted between April 2010 and March 2012 using Giant Metre wave Radio Telescope facility at Pune, India for the whole sky visible from the observatory. Its resolution is significant comparable to existing centimetre surveys despite being a meter wavelength survey- in fact it is at present the highest resolution survey below 200 MHz! [25] There are unique challenges in processing of high-resolution radio images at low frequencies due to instrumental instabilities, Radio Frequency Interference, Direction Dependent ionospheric delays etc. Often compromises are made for timely release of images only to be reprocessed whenever there are technical improvements in algorithm, knowledge of primary beam etc only to witness significant improvement in dynamic range through better RMS flux and increased identification of sources. Recently GMRT has been upgraded and there is public release of a upgraded GMRT continuum processing pipeline with hope of promoting open science. It is being called ‘CAPTURE’: A “CASA Pipeline-cum-Toolkit for Upgraded Giant Metrewave Radio Telescope data REDuction uGMRT-pipeline” [29]. It promises several benefits and it should equally work with legacy GMRT data.

We have collected TGSS raw data from GMRT archive accessible at “<https://naps.ncra.tifr.res.in/goa/data/search>” corresponding to a well-known field with multi-wavelength data GAMA G23 [ RA= 23 h, DEC= -32.5 deg search radius= 300’]. Further data was also downloaded so that scans covering all the 29 phase calibrators and also for few phase calibrators all scans using them in TGSS were downloaded. We had to tweak settings in CAPTURE regarding flagging to image the TGSS data. First using the 9 pointings from GAMA G23 we identified 2 settings that gives best images and they worked with all other scans we downloaded so far. to We have compared flux scale and dynamic range between images we made and those available as TGSS-ADR cutout services.

It is important to note that although ADR images have undergone Direction Dependent calibration, our images are limited to only rounds of self calibrations (Direction Independent calibration) we can almost match the dynamic range of ADR. Though apparently RMS noise in our image is slightly higher but it is the flux scale accuracy which is most important. Further we can confirm that flux in our analysis is consistent to existing literature and we do identify a few cases of flux discrepancy when working

with ADR image mosaic/cutout. Although this may be expected since no pipeline (including SPAM which ADR is based on[24]) is perfect; however it makes **this work important and distinguishable from rest-**

- **We intend to establish an accurate flux density scale for TGSS and also inform any existing issues with ADR. Further no previous work has matched the flux of all 29 phase calibrators in TGSS as per own analysis and that available from ADR MOSAIC/cutout to understand flux issues.** Also the variations of flux for same phase calibrator but in different scans was investigated for atleast 5 phase calibrators.
- **Promote Open Science:**All want free publicly available pipelines for repetitive but demanding task such as raw interferometric data reduction. Because without pipelines, the science ready images/ products from raw radio interferometry data will always depend on the choices a group of researchers use to make those for themselves while other researchers will remain skeptical. **This work tested the performance of ‘CAPTURE’ pipeline at 150 Mhz with legacy GMRT data, issues were learnt and some improvements on usage was made, and we hope it will become a popular choice (being reliable, free and publicly available) to be used by all when it comes to working with legacy GMRT and upgraded GMRT continuum survey data in near future.**
- We made mosaic of GAMA G23 field, from there we have obtained Differential Source Count and spectral index. Further this work may help constrain foregrounds to probe Epoch of Reionization at redshift 8.5 since the frequency 150MHz corresponds to the redshifted H21 cm signal from the epoch.

# Contents

<b>1</b>	<b>Introduction</b>	<b>1</b>
<b>2</b>	<b>Low Frequency Radio Sky Observations</b>	<b>3</b>
2.1	Radio Telescopes . . . . .	5
2.2	Interferometry & Aperture Synthesis . . . . .	5
2.3	The Giant Metre Radio Telescope (GMRT) . . . . .	6
2.4	TIFR GMRT Sky Survey (TGSS) . . . . .	9
<b>3</b>	<b>GAMA Survey &amp; Radio Deep Fields</b>	<b>10</b>
3.1	GAMA 23 Field: Multi-wavelength Science . . . . .	11
3.2	Characterising Foreground Sources: Implication for Deep Cosmological Observations . . . . .	12
<b>4</b>	<b>Radio Interferometric Data Analysis</b>	<b>14</b>
4.1	Basic Idea . . . . .	14
4.1.1	Flux Calibration . . . . .	14
4.1.2	Phase Calibration . . . . .	15
4.1.3	Delay and Bandpass Calibration . . . . .	15
4.1.4	What happens when we don't calibrate? . . . . .	15
4.2	Self Calibration . . . . .	16
4.3	Radio Interferometric Imaging: Wide-band and Wide-field	17
4.3.1	CAPTURE vs SPAM . . . . .	21
4.4	Mosaicing and Source Catalogue . . . . .	21
<b>5</b>	<b>Analysing GAMA-23 Field from TGSS: Alternate Route</b>	<b>24</b>
5.1	Imaging using CAPTURE . . . . .	24
5.1.1	Our Images vs ADR . . . . .	26
5.1.2	Comparing between our work and ADR . . . . .	31
5.2	Flux Comparison using all Flux and Phase Calibrators in TGSS . . . . .	34
5.2.1	Our Analysis in Standard scales vs ADR . . . . .	34

5.2.2	An interesting result: Variability of flux per scan for phase calibrators . . . . .	36
5.3	Mosaic image of the 9 pointings: also covers GAMA G23 field	39
5.4	Source Catalog of the Mosaic Image . . . . .	41
5.4.1	Differential Source Count (DSC) . . . . .	42
5.4.2	Matching with NVSS catalog to Spectral Indices . .	43
<b>6</b>	<b>Conclusions and Scope for Future Work</b>	<b>46</b>

REFERENCES

# List of Figures

1.1	Radio continuum survey showing whole sky but centered on Milky way. . . . .	2
2.1	Spectrum types of different processes . . . . .	4
2.2	Basic components of a radio telescope . . . . .	5
2.3	Four types of feed. . . . .	6
2.4	Wide bandwidth of GMRT after and before upgrade. . . . .	7
2.5	Up: GMRT Antenna position This work Down: Sensitivity comparison among radio telescopes. doi: 10.18520/cs/v113/i04/707-714 . Accessed on 6th June 2021. . . . .	8
2.6	RMS noise map for TGSS in Alternate Data Release. . . . .	9
3.1	GAMA regions . . . . .	10
3.2	G23 field . . . . .	11
3.3	Different foregrounds, their relative strength & mock 21 cm signal . . . . .	13
3.4	Chronology of universe & redshift . . . . .	13
4.1	Calibration went wrong & image shows no coherence for one of our target R69D11. . . . .	16
4.2	Steps in self calibration. . . . .	17
4.3	CAPTURE’s all files and their description. . . . .	18
4.4	Settings to be supplied to ‘CAPTURE’ by user through configcapture.ini. . . . .	19
4.5	Flowchart of what ‘CAPTURE’ pipeline does. . . . .	20
4.6	Left: Simple example when mosaicing needed Right: Example of linear mosaic. . . . .	22
4.7	Hierarchy of an image in PyBDSF . . . . .	23
5.1	Left: Settings 1 and Right: Settings 2 we worked with. . . . .	25
5.2	Image of Pointing R69D13 (Date of Observation: 08jul2010)	27
5.3	Image of Pointing R69D14 (Date of Observation: 09jul2010)	28

5.4	Image of Pointing R70D11 (Date of Observation: 29Aug2010)	29
5.5	Flux, RMS & Dynamic Range Comparison between our images and ADR Mosaic	30
5.6	Ratio of Peak and Integrated Flux from our images and ADR Mosaic	33
5.7	Ratio of Flux Jy known scales vs ADR	35
5.8	Variations of Flux in PB2017 scale per scan for 1311-222	36
5.9	Variations of Flux in PB2017 scale per scan for 1419+064	36
5.10	Variations of Flux in PB2017 scale per scan for 1459+716	37
5.11	Variations of Flux in PB2017 scale per scan for 2225-049	37
5.12	Linear mosaic of 9 pointings- R69D11 , R69D12, R69D13, R69D14, R70D11, R70D12, R70D13, R70D14 & R71D11. Mosaic center (22:59:59, -31:24:50)	39
5.13	RMS Map of the MOSAIC	40
5.14	the GAMA G23 region J2000 RA (deg): 339 to 351, DEC(deg): -35 to -30	40
5.15	Differential source count	42
5.16	Correction factors per flux bin mJy.	43
5.17	Matching between our catalog & NVSS within RA,DEC error. This full 2043 rows $\times$ 12 columns catalog is available with author.	44
5.18	Histogram of spectral indices of matched 2043 sources.	45

# List of Tables

5.1	Comparing Peak Flux between us and ADR 1 per pointing.	31
5.2	Comparing Integrated Flux between us and ADR 1 per pointing. . . . .	32
5.3	Flux calibrator values in Jy from ADR & flux models . . . .	34
5.4	PB 2017 Flux values, SNR and scan details for outliers. . .	38
5.5	Table shows Differential Source Count in $Jy^{-1}Sr^{-1}$ . . . .	42

# Chapter 1

## Introduction

From the very beginning of radio astronomy in the hands of Karl Jansky, there have been continuum surveys to learn about the distribution and intensity of radio sources across the sky. It is desired that radio continuum surveys have large angular resolution enabling source identification and high sensitivity to detect emissions with low surface brightness-latest technology has guaranteed just that.[2] Continuum surveys at 150 MHz witness “Active Galactic Nuclei to be dominated by lobes instead of cores; brighter pulsar and supernovae; coherent flares from magnetically active stars; new types of transient; Galaxy clusters showing extended relics and halos etc” [25]. Among these AGN dominate the source count.

The Giant Metrewave Radio Telescope (GMRT) was used to survey the radio sky at 150 MHz between 2010 and 2012 but it remained beyond scope to publicly make products available. Later an independent team has reprocessed the TGSS data using the SPAM pipeline (includes ‘corrections for direction-dependent ionospheric phase effects’-something earlier not available) and made products available to public through project named TGSS Alternate Data Release. It is a common practice to reprocess important survey data whenever techniques become available to do so because the confidence in what we see improves- unfortunately there is no unique solution to deconvolution involved in imaging and it’s always based on a priori assumptions. Further though there are not enough documents; radio astronomers familiar with TGSS have come to believe that many extended emissions were missed in ADR release due to heavy flagging and notices flux scale issues sometimes when compared with MWA and LOFAR data which are at the same frequency as TGSS.

**Why should we learn about flux scale accuracy in ADR?** The high resolution and all sky coverage makes TGSS very important for science. However from raw data to finally science ready images or products is a daunting task in itself, then astronomers/scientists need to do the actual scientific investigations from there. Hence, the efforts of ADR team in making science ready images, catalogues are well appreciated and researchers world wide will be working with them. However, this means any flux discrepancy in the ADR or any other issues will occasionally get into the scientific results and will take very long to identify and or correct. This work involves reanalysis of the TIFR GMRT Sky Survey (TGSS) of an area of sky (preferably which has been already well studied in multi wavelengths) using an alternate approach than the TGSS-Alternative Data Release (TGSS ADR 1). One of the major aim of this work is to investigate issues with the accurate flux density scale and explore ways to quantify

it. This alternate analysis may provide better sensitivity in the resultant calibrated data and images. This, in turn, may improve the image fidelity and dynamic range allowing serendipitous discoveries!

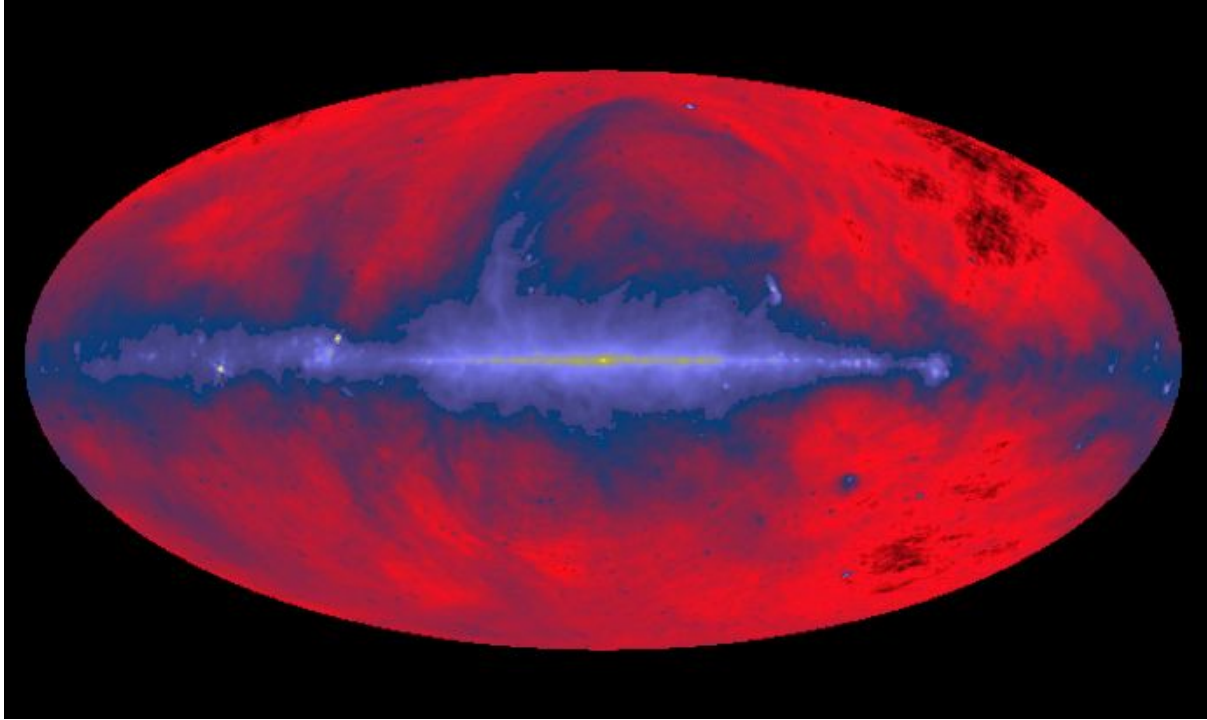


Figure 1.1: Radio continuum survey showing whole sky but centered on Milky way.  
<http://ircamera.as.arizona.edu/NatSci102/NatSci102/text/multiwavelength.htm>  
Accessed on 6th June 2021.

In this thesis, chapter 2 intends to make one familiar with radio astronomy. Most of the time it is seen that because general audience often restricts themselves to only optical astronomy and thinks that it is all of astronomy. The reason mainly is pretty pictures of the universe and ease to get in touch with an optical telescope. It is difficult to make and access something like a radio telescope and they do not produce instant images like the optical telescopes. In this chapter, we will discuss the beginning of the radio astronomy and how it opened the door to the undiscovered universe. We will emphasize the scientific significance of the discoveries made at radio and microwave wavelengths. Then, we learn about the basic components that make up radio telescope, a technique called interferometry that makes it possible to have good resolution images at long radio wavelengths. Then we proceed to understand the Indian GMRT telescope since we are working with data from this telescope only. Further technical details of TGSS & ADR are visited. Few relevant topics of extra galactic science are covered. Chapter 3 we talk about GAMA surveys and fields especially GAMA G23 since we decided to download data for this region only for the project. Next Chapter 4 is about getting images from raw interferometry data- briefly introduces the types of calibration, pipelines and finally takes us to important topic CAPTURE vs SPAM since all our images are reduced from raw data using CAPTURE pipeline only. Next in Chapter 5 we are ready to give details of methodology, results and discussions. Finally in Chapter 6, we conclude the thesis in light of future work that should follow.

## Chapter 2

# Low Frequency Radio Sky Observations

In old times the only source of astronomical study was the visible photons coming from the outer space which was known as optical astronomy, which has the wavelength range from 0.4 to 0.8 microns. Since the past 50 years, new branch of astronomy known as radio astronomy has become very handy, especially after world war II when radio engineers worked with radar technology and its interference which has wavelength range from 1cm to 10m. Karl Jansky discovered the radio signals coming from the extraterrestrial sources for the first time. While working at bell laboratories, he would try to locate the source of static noise that interfered with radio reception at wavelengths of 14.6m and 10m. While some of the sound was coming from nearby thunderstorms, some was coming from distant sources. By recording the data over a year, he concluded that the signal was of extra-terrestrial origin. [36]

**Radio Window:** Almost all celestial objects including planets emit some radio waves. Earth's atmosphere is opaque to most wavelengths shorter than ultraviolet, those between infrared and microwaves, and long radio waves. So, one relies only on short-wave radio to learn about the universe using our Earth-bound instruments. These frequency ranges that pass through the atmosphere are referred to as the radio window. The radio window consists of frequencies between 5 MHz and 30 GHz. The radio window expands or shrinks depending on atmospheric conditions.

**Radio sources** produce either **continuum radiation or line radiation**. Continuum radiation covers a very broad range of wavelengths and may be detected with a radio telescope tuned to any convenient wavelength. Processes that generate continuum radio radiation might be of thermal origin or nonthermal- Bremsstrahlung, Synchrotron. Line emission originates from transitions within atoms and molecules and may be detected across a narrow band about a particular frequency. They originate in clouds of gas in space and are detected both in absorption and in emission- the most famous is perhaps the H21 cm line due to its suitable optical depth at ISM. Summarized below [8]-

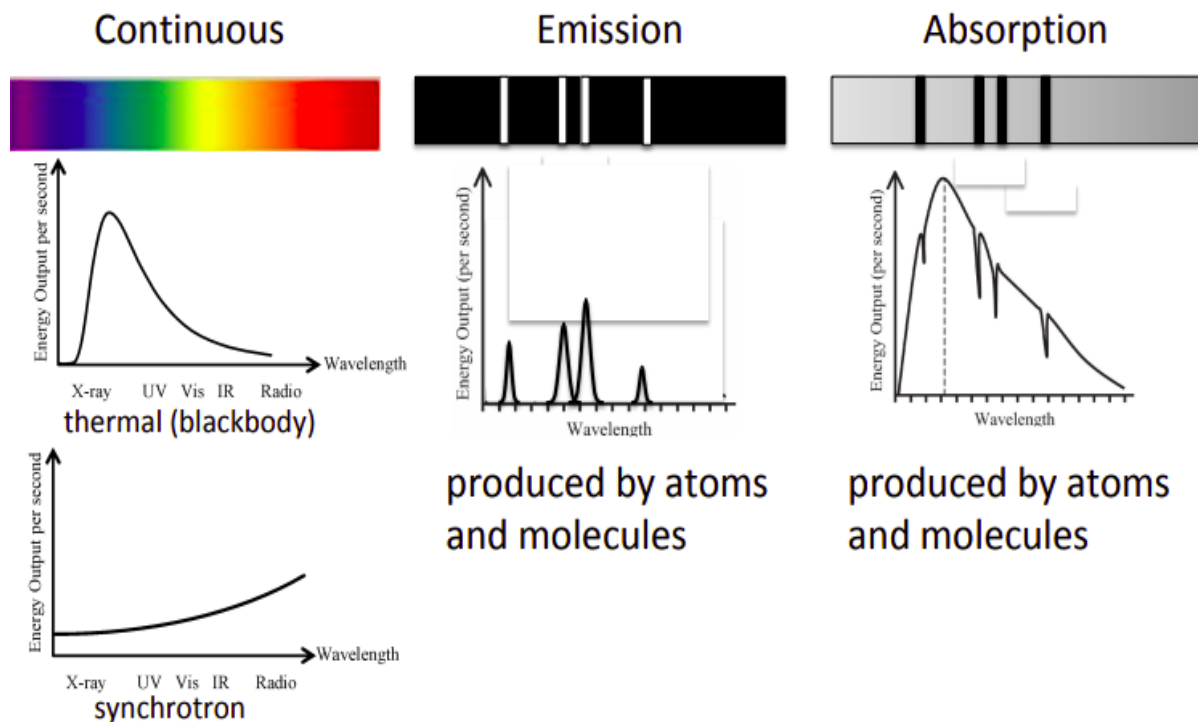


Figure 2.1: Spectrum types of different processes

<https://slideplayer.com/slide/8420113/.YLz7C0Cl7A.google>. Accessed on 6th June 2021.

DEVELOPED THROUGH A COLLABORATION OF ASTRONOMY EDUCATORS FROM CAE funded through generous contribution of AUI.

Their common physical origins:

- Thermal Emissions / Black-body spectrum. Eg: Stars.
- Free-Free Emissions/Bremsstrahlung. Eg: HI Regions.
- Charged relativistic particles in magnetic field/ Synchrotron Emission: Eg: Active Galactic Nuclei.
- Spectral-Line Absorption are lines seen against background continuum emission (E.g. HI region).
- Spectral-Line Emission: Atoms, radicals, molecules (E.g. Carbon Monoxide)

## 2.1 Radio Telescopes

[36, 9] To common folks, radio telescopes look nothing like their optical counterpart; yet they are just specialized antennas and radio receivers used to observe radio sources. The basic components of single dish radio telescope are explained below: -

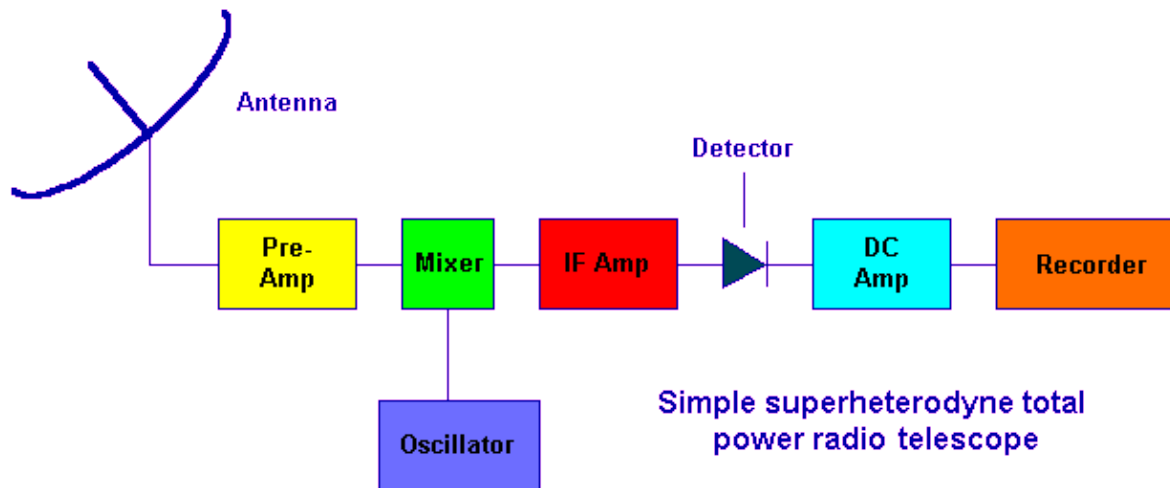


Figure 2.2: Basic components of a radio telescope

<http://www.astrosurf.com/luxorion/radioastronomy-rt.htm>. Accessed on 6th June 2021

1. “An antenna is the interface between the radio waves propagating through space and electric current moving in metal conductors.” Antenna picks up electromagnetic radiation and produce current at its terminals. When transmitting, the electricity that is fed to the antenna will make electrons “wiggle back and forth along the antenna which will produce electromagnetic radiations in the form of radio waves which travel with the speed of light” [36]. Parabolic reflectors being most common in radio astronomy but there are many kinds- monopole, dipole, loop antenna, log periodic, horn antenna etc.
2. Feed Supports are hung at the focus where multiple receivers (often a horn antenna) are installed.
3. Receiving System and Data Processing: First incoming weak signal is boosted in Low Noise Amplifier, then there is a radio telescope mixer which lowers frequency of the signal to Intermediate frequency to avoid feedback while undergoing further amplification and bandpass filtering. Finally, a detector would convert the radio frequency energy to DC.

## 2.2 Interferometry & Aperture Synthesis

The resolving power of a radio telescope can be written as

$$\theta_{res}(arcseconds) = (1.22 * \lambda * 206265)/D \quad (2.1)$$

where  $\lambda$  is wavelength (in millimetres) and D is collector diameter in millimetres and 1 pc/1 AU= 206265.

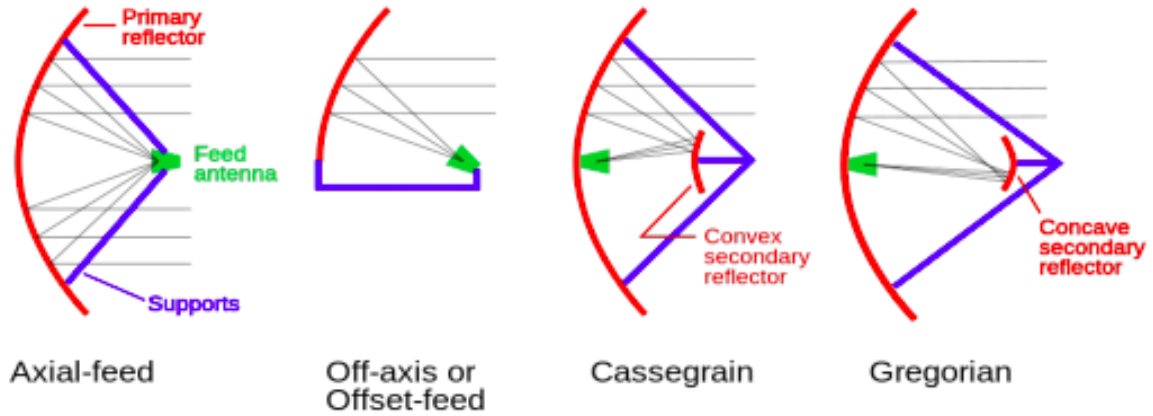


Figure 2.3: Four types of feed.

<https://en.wikipedia.org/wiki/File:Parabolicantennatypes.svg>. Accessed on 6th June 2021.

The largest single dish aperture which is steerable and also allows for safe and accurate movement is in order of 100 metres- using this formula we don't get an impressive resolution as compared to optical telescopes. Finally combining "the views of a group of antennas spread over a large area to operate together as one gigantic telescope was invented. When we combine the two offset waves, they will not overlap perfectly due to their phase shift, creating what we call interference fringes. As the Earth turns and the telescopes tilt to keep watching their source setting, the angles of their observations change. This translates to different phase delays between the waves reaching each telescope. The longer we observe, the more variations we get. The more variations we get, the more perspectives we have on the object we're observing. And the farther apart we separate the telescopes, the sharper their binocular view of the sky becomes." [9] Understanding the above requires knowledge of Fourier transformation and 'uvw' plane- a details we skip for now.

## 2.3 The Giant Metre Radio Telescope (GMRT)

"GMRT, Khodad, Pune, Maharashtra" is one of the best examples of Phased array interferometer with 30 parabolic dishes each of 45 m diameter. Its minimum and maximum baseline are 200m and 30 km allowing a resolution equivalent to 25 km aperture diameter parabolic dish. The distribution of antennas may be seen below. The central region comprises 12 out of 30 dishes in a 1x1 square km area and rest scattered in 'Y' shaped arms. Sources were observed using legacy GMRT at frequency bands- "130-170 MHz, 225-245 MHz, 300-360 MHz, 580- 660 MHz, and 1000-1450 MHz" with maximum instantaneous bandwidth of 32 MHz. The effective collecting area is 30,000 square meters at lower frequencies and 20,000 square meters at higher frequencies. GMRT supports 2 modes of operation- i) Interferometry and aperture synthesis ii) Array mode (Incoherent and coherent). [36] Recently, GMRT has been upgraded to improve the antennae's sensitivity by a factor of up to three and to keep it relevant in SKA era (See Fig 2.6 down for sensitivity comparison). What makes GMRT special-

1. SKA is based in southern hemisphere, unable to see the northern skies accessible to the GMRT.
2. SKA is a heavily subscribed object so researchers shall turn to GMRT for various other facilities when properly maintained.

Details of upgrade-

Feeds and frontend electronics which work in octave ranges of frequency have been designed for ‘seamless frequency coverage at wide bandwidths. Also improvements are made in ‘wideband optical fiber transmission scheme’ to transport the radio frequency (RF) signals from the antennas to the central receiver building, and wide bandwidth analog and digital backends at the central receiver building. The frequency bands now available with upgraded GMRT: “5080 MHz (band-1), 120–250 MHz (band2), 250–500 MHz (band-3), 550–850 MHz (band-4), 1050–1450 MHz (band-5).” [21]

See fig below for comparison of frequency bands between legacy and uGMRT.

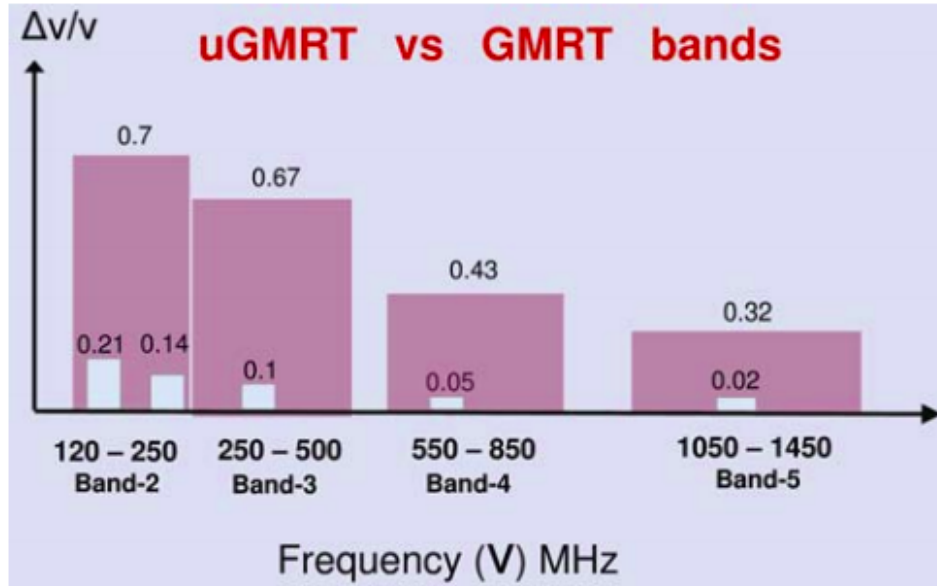


Figure 2.4: Wide bandwidth of GMRT after and before upgrade.  
doi: 10.18520/cs/v113/i04/707-714 . Accessed on 6th June 2021.

In fig 2.6 up We see GMRT ANTENNA ARE POSITIONS ‘Y’-SHAPED. WHY? To produce “a nearly circular resolution synthesized beam on the sky for a variety of integration times and for most positions on the sky.” Also this arrangement is most useful for this number of antennas (30) to connect to central power and communication located at the center. Finally, the Y-configuration makes it possible to expand and contract the array to allow for changing needs of baselines and/ resolution.[10]

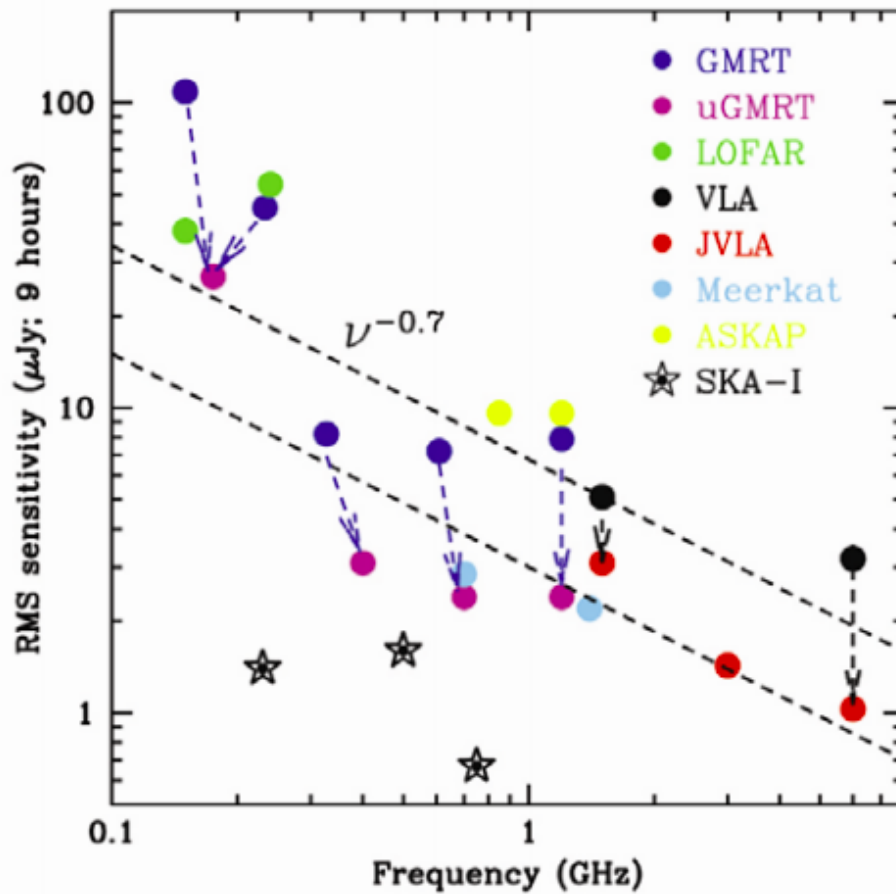
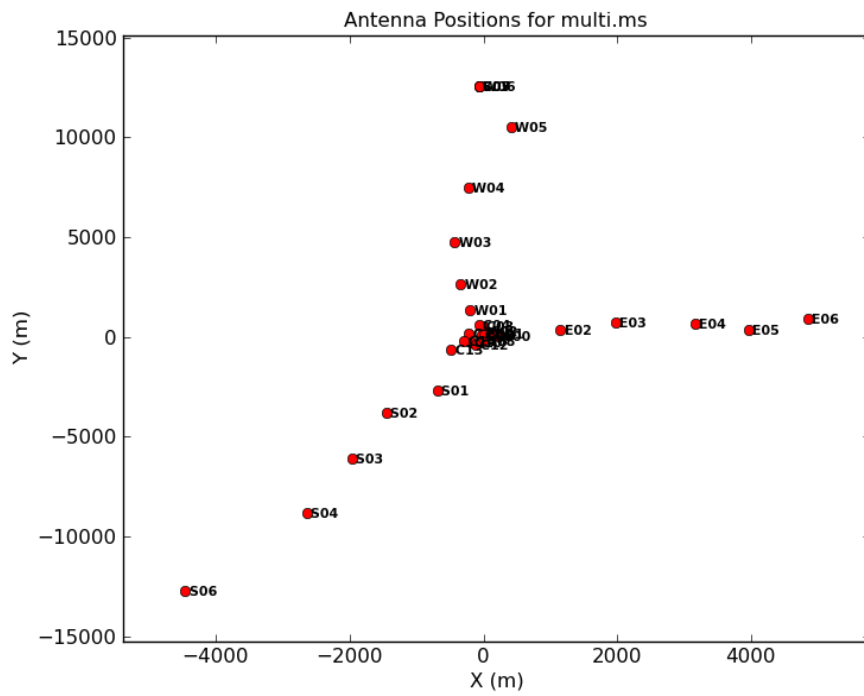


Figure 2.5: Up: GMRT Antenna position This work Down: Sensitivity comparison among radio telescopes. doi: 10.18520/cs/v113/i04/707-714 . Accessed on 6th June 2021.

## 2.4 TIFR GMRT Sky Survey (TGSS)

The Giant Metrewave Radio Telescope (GMRT) was used to survey the radio sky at 150 MHz between 2010 and 2012 but it remained beyond scope to publicly make products available. Later an independent team has reprocessed the TGSS data using the SPAM pipeline (includes ‘corrections for direction-dependent ionospheric phase effects’- something earlier not available) and made products available to public through project named TGSS Alternate Data Release. The data processing and products are described in detail in [25].

“Under the project, the following three services are publicly available-

1. TGSSADR Image Archive: 5336 mosaic images of  $5 \times 5$  square degrees over entire survey area.
2. TGSSADR Image Cutout Service: cutout images of up to  $1 \times 1$  square degree anywhere in the survey area.
3. TGSSADR Source Catalogue : contains information on 0.63 Million radio sources which have been extracted from the full survey area.

Hence TGSS ADR includes continuum stokes I images of 99.5 percent of the radio sky north of  $-53^\circ$  DEC (3.6 sr, or 90 percent of the full sky) at a resolution of  $25'' \times 25''$  north of  $19^\circ$  DEC and  $25'' \times 25'' / \cos(\text{DEC}-19^\circ)$  south of  $19^\circ$ , and a median noise of 3.5 mJy/beam. The extracted radio source catalog contains positions, flux densities, sizes and more for 0.62 Million sources down to a 7-sigma peak-to-noise threshold.” [7]

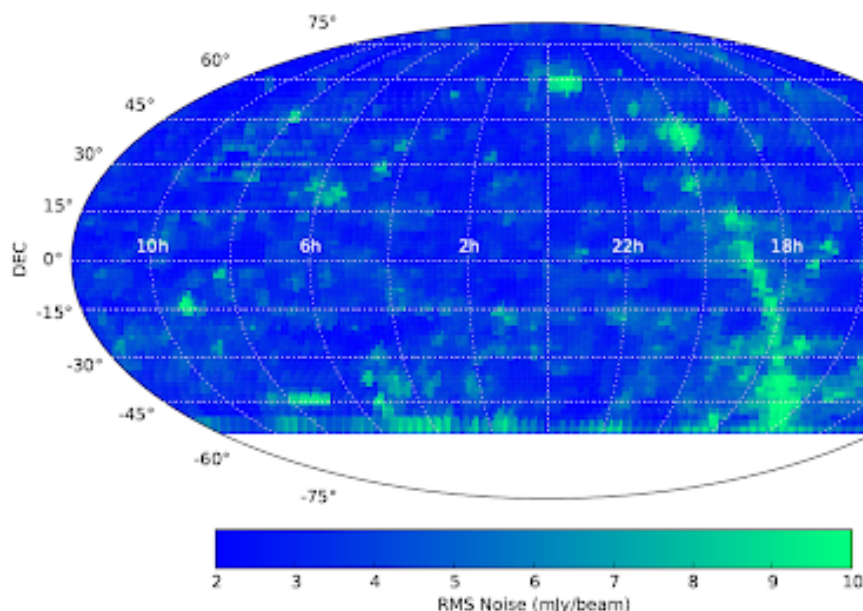


Figure 2.6: RMS noise map for TGSS in Alternate Data Release.

<http://tgssadr.strw.leidenuniv.nl/lib/exe/detail.php?id=startmedia=tgssadrrmssky.jpg>.

Accessed on 6th June 2021.

# Chapter 3

## GAMA Survey & Radio Deep Fields

The “Galaxy And Mass Assembly Survey (GAMA)” has two main sets of aims [16]:

1. galaxy distribution test the Cold Dark Matter (CDM) paradigm.
2. Study the internal structure and evolution of the galaxies themselves.

Besides learning the large-scale distribution GAMA in the long term should give us a uniform, multiwavelength and spatially resolved galaxy database built on earlier local surveys but going beyond upto covering “fainter flux levels, higher redshift, higher spatial resolution” across UV to radio wavelengths. The scientific advantages are justified by three topical issues:

1. Galaxy Structure (Driver et al. 2006 or Cook et al. 2010 or Allen et al. 2006; Gadotti 2009, Hopkins et al. 2006 ).
2. Dust attenuation (Shao et al. 2007; Choi et al. 2007; Driver et al. 2007, 2008; Masters et al. 2010).
3. The HI content (Hopkins, McClure-Griffiths Gaensler 2008, Lah et al. 2009, Johnston et al. 2007).

GAMA has executed spectroscopic survey down two magnitudes deeper than the main SDSS survey to  $r_{AB} = 19.8$ . There are five roughly equal-sized areas covering a large range in right ascension: three equatorial 60 square degree regions (G09, G12 and G15), a 50 square degree patch overlapping with the Canada France Hawaii Telescope Legacy Survey (CFHTLS) W1 (G02) and another similar size centred within the VST ATLAS survey (G23) located  $339 < RA < 351$  degrees and  $-35 < Dec < -30$  degrees.” [3].

Survey region	RA range (J2000) (deg)	Declination range (J2000) (deg)		Area (deg <sup>2</sup> )	main survey limits ( $r$ band except in G23) (mag)		
		GAMA I	GAMA II		GAMA I	GAMA II	DR3
G02	30.2 – 38.8	–	–10.25 – –3.72	55.71	–	19.8	19.8
G09	129.0 – 141.0	–1.0 – +3.0	–2.0 – +3.0	59.98	19.4	19.8	19.0
G12	174.0 – 186.0	–2.0 – +2.0	–3.0 – +2.0	59.98	19.8	19.8	19.0
G15	211.5 – 223.5	–2.0 – +2.0	–2.0 – +3.0	59.98	19.4	19.8	19.8
G23	339.0 – 351.0	–	–35.0 – –30.0	50.59	–	19.2 ( $i$ band)	–

Figure 3.1: GAMA regions

[https://www.astro.ljmu.ac.uk/ikb/research/gama\\_fields/](https://www.astro.ljmu.ac.uk/ikb/research/gama_fields/)

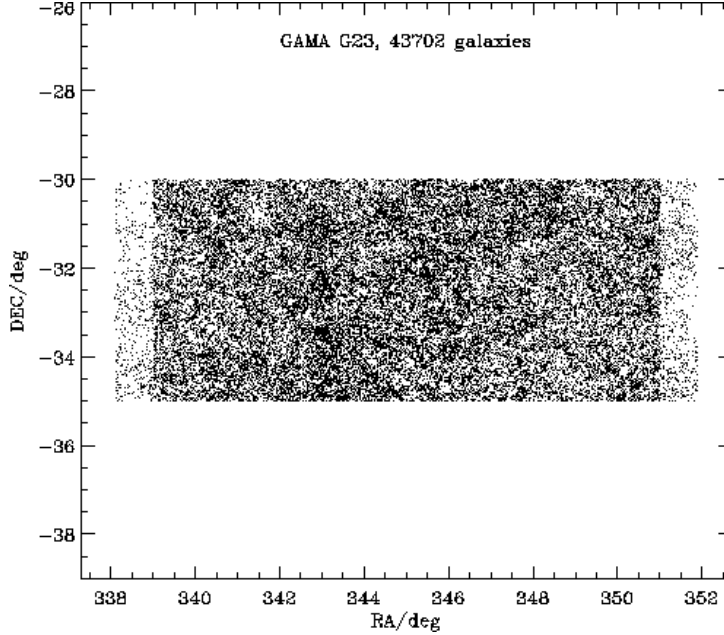


Figure 3.2: G23 field

<https://www.astro.ljmu.ac.uk/~ikb/research/gamafields/z-ra-decG23.gif>.

Accessed on 6th June 2021.

### 3.1 GAMA 23 Field: Multi-wavelength Science

[37, 17, 34, 31] Several surveys namely “Herschel-ATLAS, VST ATLAS/KiDS, VISTA VIKING and Hyper SuprimeCam” have allocated highest priority to GAMA fields. The G23 field is free from any known bright continuum sources- specifically motivated for ‘ASKAP DINGO’. ASKAP would not be suitable at the other equatorial GAMA fields which lack rotation of sky and would produce significant noisy beam width. G23 combined with ASKAP will answer “whether the cosmic H I has remained static or declined to within a factor of two over a 4 Gyr baseline”. Hence a unique multi-wavelength database for the ‘investigation of the conversion of gas into stars as a function of redshift, stellar mass, age and metallicity’ will become available. State-of-the-art group catalogue (‘like those already created for the GAMA equatorial fields by Robotham et al. [2011]’), will allow -

1. ”Investigation on how galaxy formation processes (e.g., mass–metallicity relation, SFRs, morphologies, etc) correlate with halo mass.
2. Identify different populations of AGN which in turn sample the underlying dark-matter density distribution with a different bias.
3. Separate out AGN and star-forming galaxies on either morphology for jet sources or through pure brightness temperature measurements.
4. With rich data sets we can investigate radio-loud AGN and trace the AGN activity (triggering and feedback) up to the high- $z$  Universe -- > advancement in the galaxy formation and evolution models. Progress is currently limited by the lack of wide-field, deep radio loud AGN samples that extend to high- $z$ , and so is limited only to the local Universe.” [34]

The science goals specific to TGSS are:

1. Broadening the current frequency coverage down to 150 MHz for Spectral Energy Distribution studies.
2. Obtaining high resolution images of the sources with MWA of the same region. Or we may attempt resolving structures for the low resolution MWA sources.
3. Search for MHz peak spectrum sources. [?]
4. Identify steep spectrum high-z radio sources. [26]

## 3.2 Characterising Foreground Sources: Implication for Deep Cosmological Observations

First let us begin with "Differential Source Count of extragalactic sources at radio wavelengths is important to explore the nature and evolution of radio sources ([35]; [28]; [12]; [27]; [38]) and thus to probe cosmological questions." Radio source counts have also established the "emergence of new classes of radio sources, distinct from classical radio galaxies" ([19]; [38]; [14];[12]). Haarsma and others in year 2000, [22] demonstrated how to measure the star formation history of the universe unaffected by dust extinction using source counts at 1.4 and 4.8 GHz . We note that establishing the existence and properties of new classes of radio sources is made easier if counts at several frequencies are available, so that the average spectral indices and other properties of the sources can be determined. Obtaining Radio Source Counts at multiple wavelengths has become increasingly important especially for modeling the foreground noise (see fig. 3.3) that extragalactic radio sources introduce into images of weak signals such as Epoch of Reionization which are to be probed with redshifted H21 cm line. Since a deep multiwavelength database for G23 field is visioned to become available, choosing this field has some advantages. Although in our present work we cannot go very deep due to short observation time of TGSS, however characterizing foregrounds at 150 MHz will help us detect weak H21 cm line (1420 MHz) at redshift  $z = 8.5$  approx. This in turn will enable us to observe first stars, first galaxies etc belonging to Epoch of ReIonization at that redshift. Epoch of Reionization itself is a very interesting period in chronology of universe when there is a transition of ionization fraction from neutral atomic hydrogen to ionized plasma . (See fig. 3.4) [23]

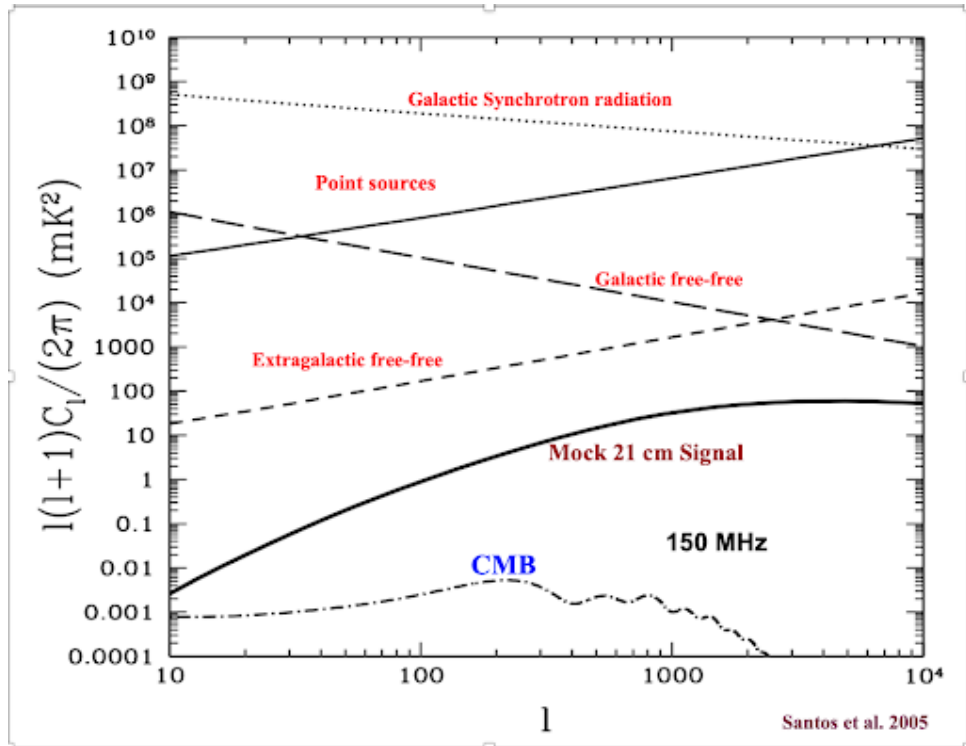


Figure 3.3: Different foregrounds, their relative strength & mock 21 cm signal

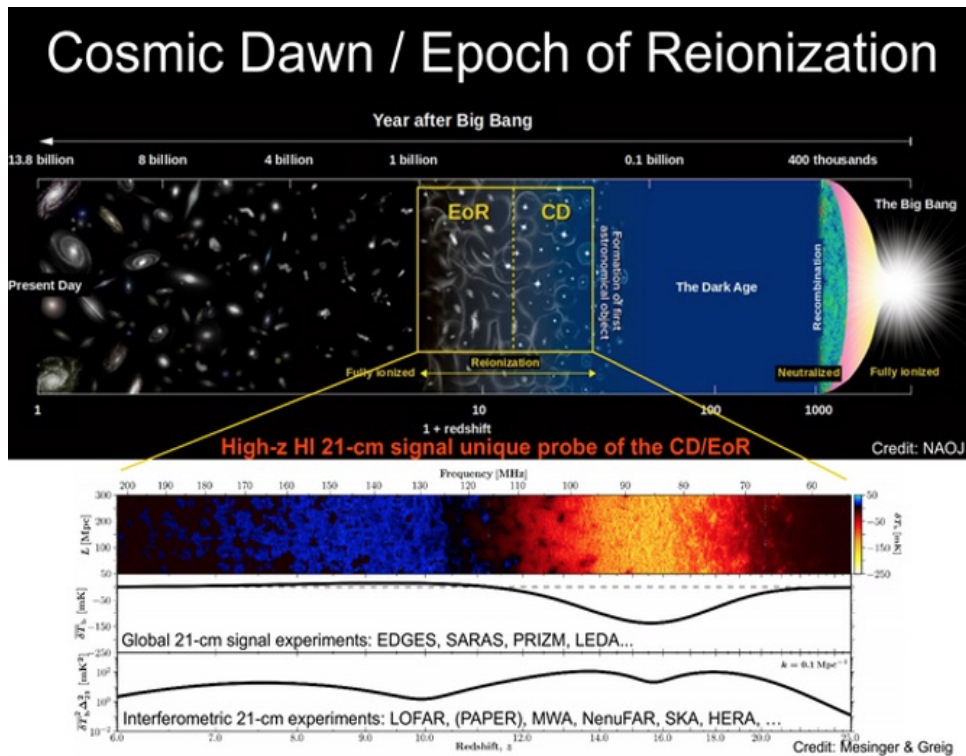


Figure 3.4: Chronology of universe & redshift

# Chapter 4

## Radio Interferometric Data Analysis

### 4.1 Basic Idea

[30, 5] Interferometers measure “visibilities”: the amplitude and phase information of the cross-correlated signals between pairs of antennas. The true visibility is corrupted by many effects: –

1. Antenna Based Effects: “Atmospheric attenuation, Radio ‘seeing’, Variable pointing offsets, Variable delay offsets, Electronic gain changes, Electronic delay changes, Electronic phase changes.”
2. Baseline Based Effects: “Radiometer noise, Correlator malfunctions, Most Interference signals.”

We calibrate these data by determining the complex gains (amplitude and phase) and the frequency response (bandpass) for each antenna. Corrected visibility is believed to be related to source brightness through Fourier transform. So, we have 3 types of calibration-

#### 4.1.1 Flux Calibration

The correlator combines signals from the antennas into visibilities. The signal strength and phase are however in relative terms. In order to get absolute flux density from sky visibilities one observes a calibrator along with other observations in the scheduling block. A flux calibrator is a source with very well-known flux density value at the observed frequency and ideally strongest source in field of view filling 95 percent beam area; also the flux calibrator should show no time variability. The visibilities of this flux calibrator can then be re scaled for to the known flux value at the observed frequency. Then visibilities for other observations are simply matched (‘bootstrapped’) using the relative scale and the absolute flux density of the flux calibrator. However at the low radio frequencies (150MHz) we are dealing with, there are many challenges:

- Large wavelength gives to large Field Of View containing many strong sources.
- At low declinations Galactic synchrotron radiation also gets stronger at low frequencies and may flood the already weak signals from sources.

However with GMRT the choice of flux calibrators are mostly always among 3C48, 3C147 and 3C286.

### 4.1.2 Phase Calibration

The time variability of atmosphere through which the wave front passes is the culprit here and it becomes necessary to 'Calibrate the Amplitude and Phase vs. Time of Each Antenna'. The best phase calibrator will have the following properties-

- sufficiently bright few hundred mJy/beam
- preferably point like or known structure
- **most importantly observed within about  $15^\circ$  (for low frequency observations) of target sources.**

The difference between choice of flux and phase calibrator is Phase calibration need not to be brightest but should be closely located to target source so that we can assume the same atmospheric corruption occurred to our target as the phase calibrator-not strictly true and this leaves residual errors which may be improved by self calibration!

### 4.1.3 Delay and Bandpass Calibration

Small deviations such as those in inaccurate antenna position, timing etc from the calibrator model are noticeable as a time-constant linear phase slope (called 'delay') as function of frequency in the correlated data for a single baseline. This delay depends on Intermediate Frequency but same for all sub bands or spectral windows in base band. Averaging in frequencies without delay correction for a continuum image causes "decorrelation of the continuum signal and is not a correct representation of the sky". There are also small impurities in the frequency amplitude and phase response as function of frequency (independent of the delay) due to electronics band pass. These are a property of the sub band and sub band's location in baseband. Uncorrected bandpass causes incorrect relative amplitudes and phases hampering the spectral representation of the sky. Averaging these uncorrected impurities over frequency into a continuum image limits the achievable signal to noise and dynamic range. So the need to 'Calibrate the Amplitude and Phase vs. Frequency of Each Antenna' arises. The flux calibrator often doubles up as bandpass calibrator. The delay and bandpass calibration is determined on a short time interval on a strong source in order to achieve high signal to noise for the solution without including the time dependent variations.

### 4.1.4 What happens when we don't calibrate?

Without flux calibration, flux density will be in arbitrary scales which none can use! For not doing phase and delay plus bandpass calibration, there will be no coherence and source would be echoed throughout the image to an extent where it cannot be visually identified.

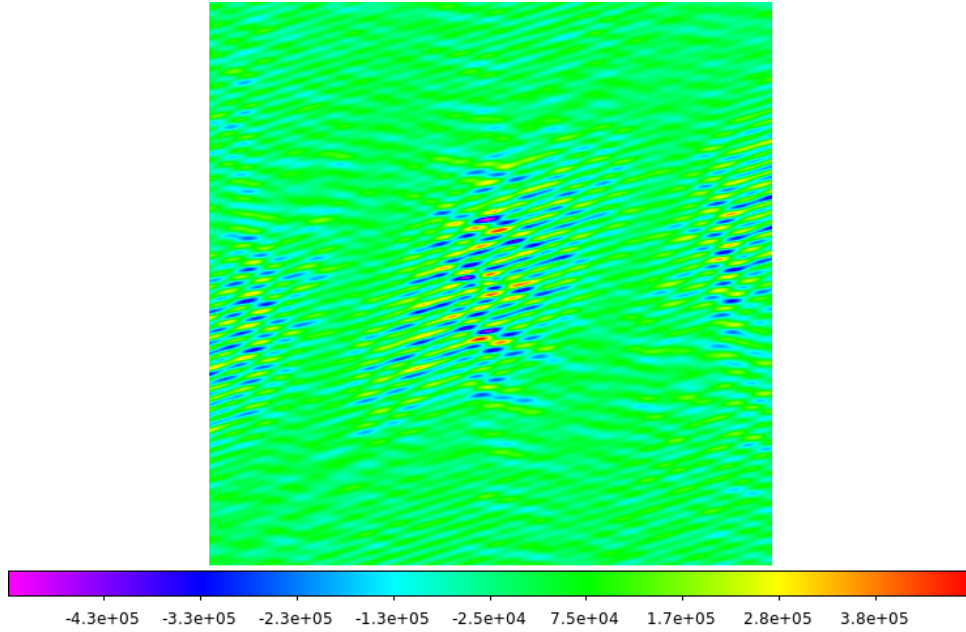


Figure 4.1: Calibration went wrong & image shows no coherence for one of our target R69D11.

## 4.2 Self Calibration

The assumption that corrections derived for the calibrator sources apply equally well to target sources depend on element of luck because atmosphere is variable, the target is observed at different elevation and time, how well we know electronics etc. So even after initial calibration there are often residual phase and amplitude errors- we resort to ‘self-calibration’ in which we iteratively use the existing model created during imaging the data itself. This works whenever sufficient visibility data are obtained: the system of equations is generally over-constrained for the number of unknowns . “For an array of  $N$  antennas, at any given instant, there are  $N(N-1)/2$  visibility data, but only  $N$  gain factors. For an array with a reasonable number of antennas,  $N > \tilde{8}$ , solutions to this set of coupled equations converge quickly.” Caveat: Self calibration won’t work if the corruptions to true visibilities are not antenna based- this is often the case with high dynamic range images with baseline-based factors. [30]

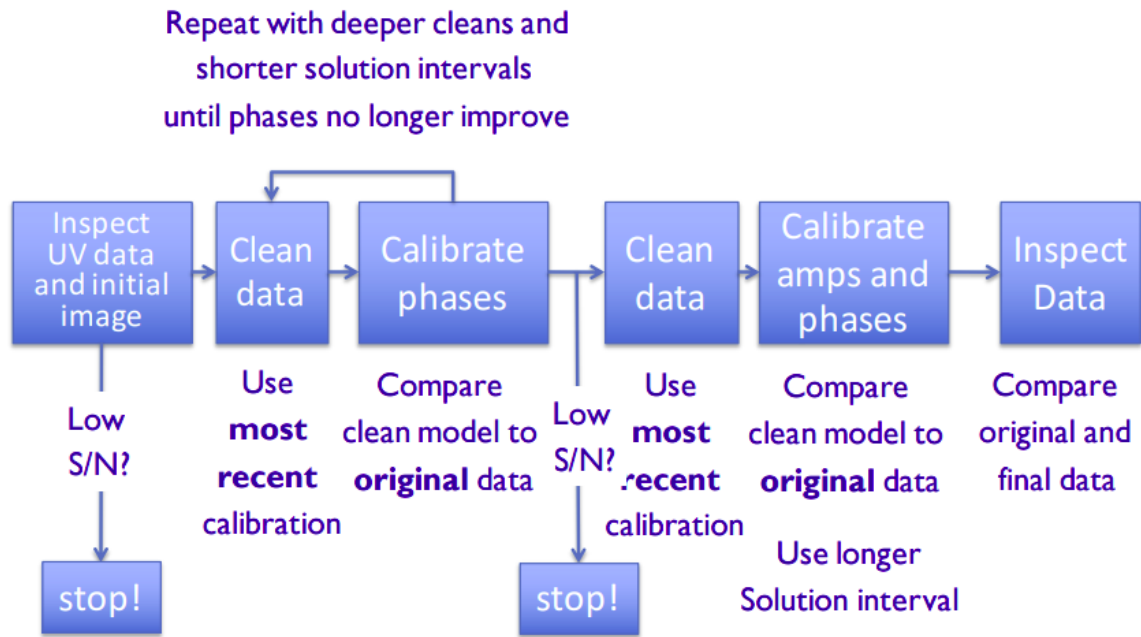


Figure 4.2: Steps in self calibration.

A. Kepley and C. Brogan, “When, why, and how to do self-calibration Sabrina Stierwalt.” <https://science.nrao.edu/facilities/alma/naasc-workshops/nrao-cd-wm16/SelfcalMadison.pdf>. Accessed on 6th June 2021.

### 4.3 Radio Interferometric Imaging: Wide-band and Wide-field

“The Astronomical Image Processing System is a software package for calibration, data analysis, image display, plotting, and a variety of ancillary tasks on Radio Astronomical Data from the National Radio Astronomy Observatory.” In early nineties it was rewritten almost in C++ to replace already aging AIPS software. The AIPS++ has now become CASA. [1]

The Common Astronomy Software Applications package (CASA) is the primary data processing software for the ALMA, Karl G. Jansky VLA, but due to its versatility other radio telescopes like GMRT, MWA and ATCA benefit in interferometric and single dish data reduction. Also, CASA provides flexibility to process the data via task interface or as a python script- this is of great help! Continuum imaging reducing from raw data is a lengthy process but some part of it is routine and repetitive. So we can write a pipeline. This offers the benefit of open science and independent verification of results as everyone would just need to agree upon settings. Without a pipeline everyone will differ in flagging and calibration strategies! Also human errors are reduced and parallel processing is encouraged.

I wish to name and compare two continuum reduction pipelines for radio astronomy for GMRT telescope -

1. “SPAM: Source Peeling and Atmospheric Modeling. (<http://www.intema.nl/doku.php?id=huibintemaspam>)”

- Python/C implementation based on AIPS functionality accessed through Parsel-Tongue interface (Kettenis+ 2006)
  - Limited support for wide-band and polarization observations.
  - A multi-layer model is available to better represent the 3D ionosphere.
  - Integrated into robust, end-to-end data processing pipeline for GMRT (and VLA) low-frequency observations, producing (near-) science-ready data products that rival manual efforts.
  - Pipeline has been successfully applied to 100’s of GMRT observations including those of TGSS. Calibration and imaging loop. [24]
2. “CAPTURE: A CASA Pipeline-cum-Toolkit for Upgraded Giant Metrewave Radio Telescope data REduction uGMRT-pipeline.

It is a python program that uses tasks from the NRAO Common Astronomy Software Applications (CASA) to perform the steps of flagging of bad data, calibration, imaging and self-calibration. The salient features of the pipeline are:

- Fully automatic mode to go from the raw data to a self-calibrated continuum image.
- Specialized flagging strategies for short and long baselines that ensure minimal loss of extended structure.
- Flagging of persistent narrow band radio frequency interference (RFI).
- Flexibility for the user to configure the pipeline for step-by-step analysis or special cases (‘toolkit’).
- Analysis of data from the legacy GMRT.” [29]

I present here more details on how to use CAPTURE here as my current work revolves about it.

File	Description
<code>config_capture.ini</code>	Configuration file.
<code>capture.py</code>	Code for processing.
<code>ugfunctions.py</code>	Python functions.
<code>vla-cals.list</code>	List of calibrator names
<code>listscan, gvfits</code>	Precompiled binaries for Ita to FITS conversion.

Figure 4.3: CAPTURE’s all files and their description. [29]

Parameter	Value	Description
fromlta	= True	Convert lta file to FITS.
fromfits	= True	Convert FITS to MS.
frommultisrcms	= True	When working with a multi-source MS file.
findbadants	= True	Find bad antennas.
flagbadants	= True	Find and flag bad antennas.
findbadchans	= True	Find bad channels within known RFI affected frequency ranges.
flagbadfreq	= True	Find and flag bad channels.
flaginit	= True	Do initial flagging.
doimtcals	= True	Calibrate the data.
doflag	= True	Flag on the calibrated data.
redocal	= True	Re-do the calibration.
dosplit	= True	Split the target source data.
flagsplitfile	= True	Flag the target source data.
dosplitavg	= True	Average target source data in frequency.
doflagavg	= True	Flag on the frequency averaged data.
makedirty	= True	Make a dirty image.
doselfcal	= True	Run imaging and self-calibration.
ltafile	= file.lta	Name of the lta file.
gcbinpath	= ./listscan./gcbfits	Path to the listscan and gcbfits executables.
fits_file	= TEST.FITS	Name of the FITS file.
msfilename	= test.ms	Name of the multi-source MS file.
splitfilename	=	Name of the split file if available.
splitavgfilename	=	Name of the frequency averaged file if available.
setquackinterval	= 10	Time in seconds to flag at the beginning and at the end of each scan.
ref_ant	= C00	Provide reference antenna name. Note that the antenna number will not work.
clipfluxcal	= 0.0,80.0	Clipminmax levels in Jy for flux calibrator.
clipphasescal	= 0.0,60.0	Clipminmax levels in Jy for the secondary calibrator/s.
cliptarget	= 0.0,30.0	Clipminmax in Jy for target source.
clipresid	= 0.0,10.0	Clipminmax in Jy for residual column used only during self-calibration.
chanavg	= 50	Number of channels to average. Choose in order to avoid bandwidth smearing.
imcellsize	= 1.0arcsec	Cell size for imaging.
imsize_pix	= 7000	Image size in pixel units.
scaloops	= 8	Total number of self-calibration loops (including both phase-only and amplitude and phase).
mJythreshold	= 0.01	A setting equal to the expected rms in mJy is found to work fine.
pcaloops	= 4	Number of phase-only self-calibration loops; should be <= scaloops.
scalsdints	= 8.0min, 4.0min, 2.0min, 1.0min, 4.0min, 2.0min, 1.0min, 1.0min	List of "solint"s for the task gained in self-calibration.
niter_start	= 1000	Number of iterations for the first imaging in the self-calibration loop.
use_nterms	= 2	The nterms parameter used in tclean.
useprojpl	= -1	Number of w-projection planes; -1 implies that it is determined internally in tclean.

Parameter	Value	Description
uvrascal	=	UV-range cutoff used in calibration (not tested).
uvrascal	=	UV-range cutoff used in self-calibration (not tested).
target	= True	Always set to True.
usetclean	= True	Always set to True.

Figure 4.4: Settings to be supplied to ‘CAPTURE’ by user through configcapture.ini.

[29]

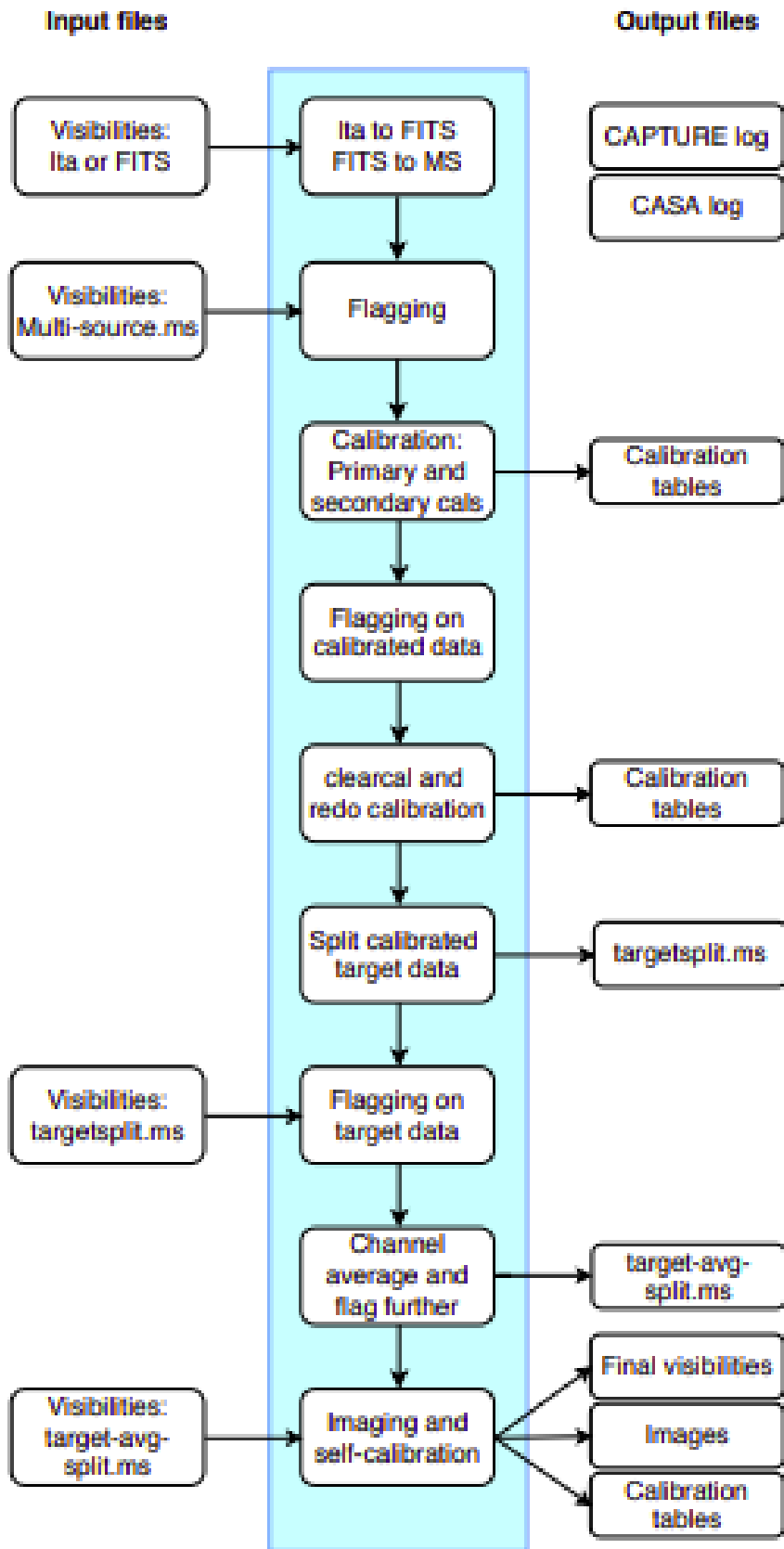


Figure 4.5: Flowchart of what 'CAPTURE' pipeline does.

[29]

### 4.3.1 CAPTURE vs SPAM

CAPTURE and SPAM are both publicly available. In order to decide which one to use when; one may look into these differences-

1. SPAM does peeling/Direction Dependant calibration but not CAPTURE .

However we may use CAPTURE+DDF-kMS pipeline (Kale, Shimwell, Tasse) or CAPTURE+CUBICAL pipeline (Kale+GEMSS collaboration) for DD calibration. Flagging percentage difference is not known, but privately it appears that SPAM flags heavily while CAPTURE used as a toolkit allows for customized flagging strategy. CAPTURE allows better handling of wideband and widefield effects for uGMRT data using algorithms such as “w-projection and multi frequency synthesis” in CASA. SPAM has some options to process uGMRT wideband data.

2. SPAM does not support the processing of large fractional bandwidths ( $df/f > 0.2$ ) in one run, but instead the bandwidth can be split up into smaller chunks (sub-bands) that can be processed independently.

“If done carefully, the calibrated output visibilities of SPAM pipeline run on multiple sub bands can be jointly imaged with a wideband imager (WSClean) as a final step. This approach has produced good results when applied on bands 3 (250-500 MHz) and band 4 (550-850 MHz) data. Processing band 2 data (120-250 MHz) has given mixed results. Since there is not yet a good way to apply the wideband primary beam corrections, this approach only works for observations where the target’s angular size is small with respect to the primary beam size ( $size < 0.1 * FWHM$ ).”  
[4]

## 4.4 Mosaicing and Source Catalogue

Why MOSAIC? A single pointing may cover only a small portion of sky. Often source locations are not known or are scattered over a region comparable to primary beam or may be the size is comparable to Field of View or unknown we will need to mosaic a number of pointings to view a larger area.

Types of MOSAIC -

- Linear combinations of individual deconvolved maps.
- Joint deconvolution of single combined dirty map from individual dirty maps.
- Widefield imaging involves deconvolution of single dirty map from combining visibilities from all pointings in uv plane.

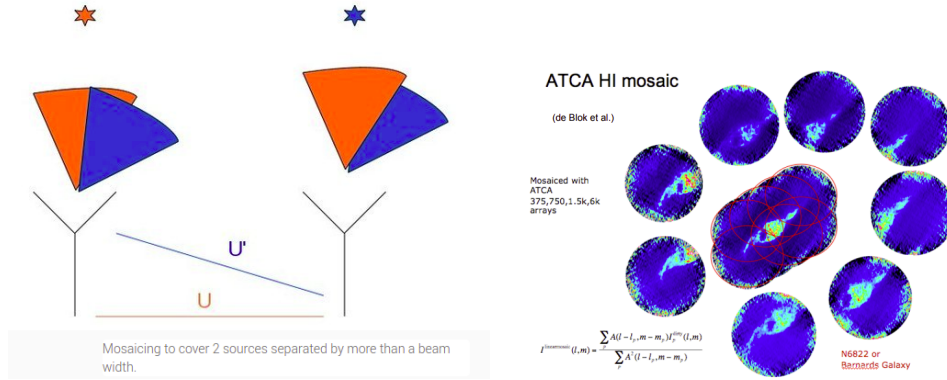


Figure 4.6: Left: Simple example when mosaicing needed Right: Example of linear mosaic.

Let us summarize advantage & disadvantage of each type of mosaicing.

Type; Available Tool	Advantages	Disadvantages
Linear Mosaicing; CASA toolkit im.linear_mosaic	For High Dynamic Range imaging each pointing can be calibrated best	Depth cannot exceed that of individual pointing, Not great at shorter spacings.
Joint deconvolution; CASA clean task imager mode 'mosaic' ftmachine='ft'	More large scale structure recovered since all uv information is used per overlap	Have to start with very good model.
Widefield imaging; CASA clean task imager mode 'mosaic' ftmachine='mosaic'	When there are many pointings centres i.e. on the fly interferometry	Computationally intensive

From the mosaic or individual pointings, to do science, one will want to identify and catalog all sources with their parameters like integrated flux, peak flux, error in flux, their position etc. So source extraction software will be used. How they work is by fitting gaussians (single or multiple) to source pixels. Most radio images of deep fields are expected to primarily consist of point sources or slightly extended which remain convolved with main lobe of the dirty beam (which is kind of gaussian). Now for extended sources shapelet and/or wavelet decomposition may be useful in place of Gaussian. In this work we use PyBDSF (the Python Blob Detector and Source Finder). Very simply it works by identifying 'Islands of emission' from image which are decomposed into Gaussians. Several Gaussians may be grouped and identified as one source. [?]

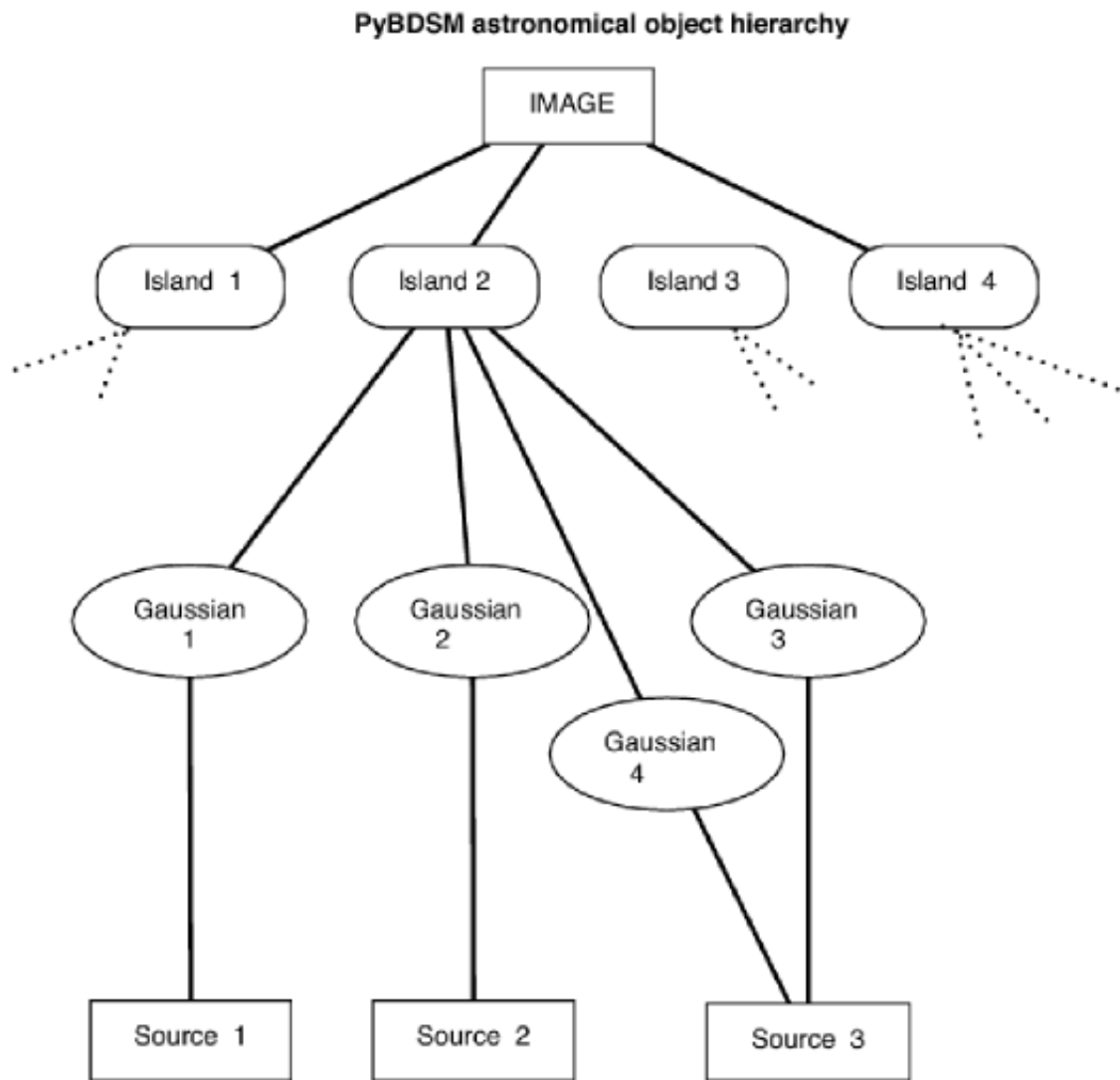


Figure 4.7: Hierarchy of an image in PyBDSF  
<https://www.astron.nl/citt/pybdsf/images/pybdsfmanualdia.png>.  
Accessed on 6th June 2021.

# Chapter 5

## Analysing GAMA-23 Field from TGSS: Alternate Route

### 5.1 Imaging using CAPTURE

Low frequency radio astronomy data at 150 MHz has significant challenges while imaging compared to the higher bands. When we started with CAPTURE with all default flagging and calibration steps to be ‘True’, we were making the data undergo Flagging then Calibration then Flagging then again redo Calibration then splitting of calibrated visibility and then again there will be flagging for the target data and then averaging. CASA seems to flag at every stage more than necessary and this entire process costs above 90% of the data to get flagged and so when we imaged the leftover, we see not meaningful images in our particular cases with TGSS. However we can confirm that leaving the default settings allows us to image even at 150 MHz if observing durations are higher. And for higher bands default settings do work fine and are already validated in ‘CAPTURE ’paper. By carefully studying the log we figured out two settings which will perform flagging only once before splitting of calibrated data. The difference between the two settings are that :

Settings 1 : initial flagging then initial calibration and no redo calibration.

Settings 2: No initial flagging but initial calibration then flagging and redo calibration.

General observation is settings 2 causes a little more flagging which is proven useful with raw data for which settings 1 seem not to work well. For all data downloaded so far, we could easily get done with just these 2 settings.

```

findbadants = False      findbadants = False
flagbadants = False     flagbadants = False
findbadchans = False   findbadchans = False
flagbadfreq = False    flagbadfreq = False
flaginit = True         flaginit = False
doinitcal = True        doinitcal = True
doflag = False          doflag = True
redocal = False         redocal = True
dosplit = True          dosplit = True
flagsplitfile = False  flagsplitfile = False
dosplitavg = True       dosplitavg = True
doflagavg = True        doflagavg = True

```

Figure 5.1: Left: Settings 1 and Right: Settings 2 we worked with.

Additionally there is also option to select uv range cutoff to be used during calibration and self calibration which we set to  $> 1000$  wavelengths and  $> 750$  wavelengths judging from our data in amp, phase vs uv wave. We truly hope that all users shall similarly be able to find out the inputs that will work for their raw visibility files if the default example settings for the band which comes with CAPTURE don't work well.

Further we took the opportunity to add functionalities in CAPTURE such as the availability to split out flux and phase calibrator visibilities and / or target visibilities - for this reason one has to set True 'dosplitcal' and / or 'dosplittar' found in 'basic' input section in capture\_config.ini file. Also one now has the option to choose among any flux standard that is available with the setjy of the CASA version one is using by simply writing the name at the input 'standard' also found in casa\_config.ini file. Example: standard=Perley-Butler 2017 or standard=Scaife-Heald 2012 etc.

One unnoticed improvement we made: Delay calibration is now done with the flux calibrator which is flagged the least when multiple are present instead of the first one in the list.

We begin by downloading all raw GMRT SOFTWARE BACKEND data files which overlaps within search radius 5 degrees of GAMA-G23(23:00:00.0,-32:30:00 J2000). This way we found total 9 pointings covering G23 from three data files - 18\_031\_08jul2010\_gsb.lta, 18\_031\_09jul2010\_gsb.lta & 18\_031\_29aug2010\_gsb.lta . The Centre of the 9 pointings each sized 6.67 by 6.67 sq degree are tabulated below:

<b>Pointing</b>	<b>Centre RA,DEC in deg</b>
R69D11	340,-33.64
R69D12	342.5, -31.93
R69D13	340.0, -30.25
R69D14	342.5, -28.60
R70D11	345.0, -33.64
R70D12	347.5, -31.93
R70D13	345.0, -30.25
R70D14	347.5, -28.60
R71D11	350.0, -33.64

Below we mention our imaging parameters in CAPTURE for all the 9 pointings: We averaged Channels by 4 , any more would induce smearing. Image cell size was 4 arc second to have 5 pixels per beam (resolution approx 20 arcsecond). We worked out Half Power Beam Width due to primary beam to be 11 184.14" and taking FIRST NULL at twice HPBW or 22368.28". Now this makes FIRST NULL/ PIXEL SIZE=5592.07. CASA does not require strictly power of 2 but its Fast Fourier Transform engine works efficiently if the number of linear pixels in a given image axis is multiple of 2, 3 and 5 alone. Image size in pixels \* pixels was chosen to be 6000\*6000. Atleast 4 phase only, in addition we attempted 1 or 2 amp phase self calibration loops if we perceived improvements. The solution intervals for each successive iteration are as follows 8.0min,4.0min,2.0min,1.0min,4.0min & 2.0min.

### 5.1.1 Our Images vs ADR

**Visually** We show sample images for 3 pointings out of total 9, one each from three raw GMRT SOFTWARE BACKEND data files 18\_031\_08jul2010\_gsb.lta, 18\_031\_09jul2010\_gsb.lta & 18\_031\_29aug2010\_gsb.lta which overlaps within search radius 5 degrees of GAMA-G23 (23:00:00.0,-32:30:00 J2000).

Up: Our Analysis CASA/CAPTURE Down: TGSS ADR MOSAIC

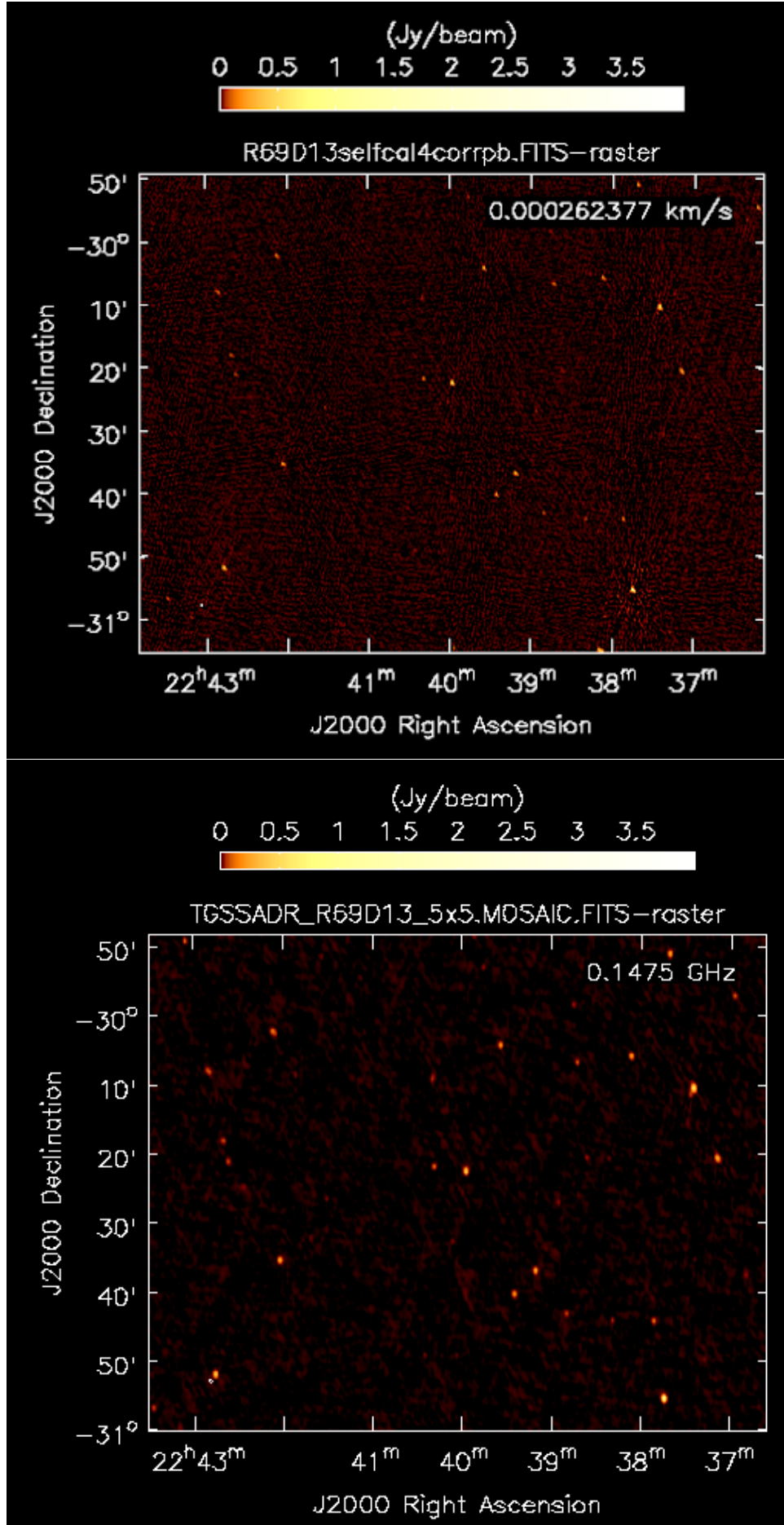


Figure 5.2: Image of Pointing R69D13 (Date of Observation: 08jul2010)

Up: Our Analysis CASA/CAPTURE Down: TGSS ADR MOSAIC

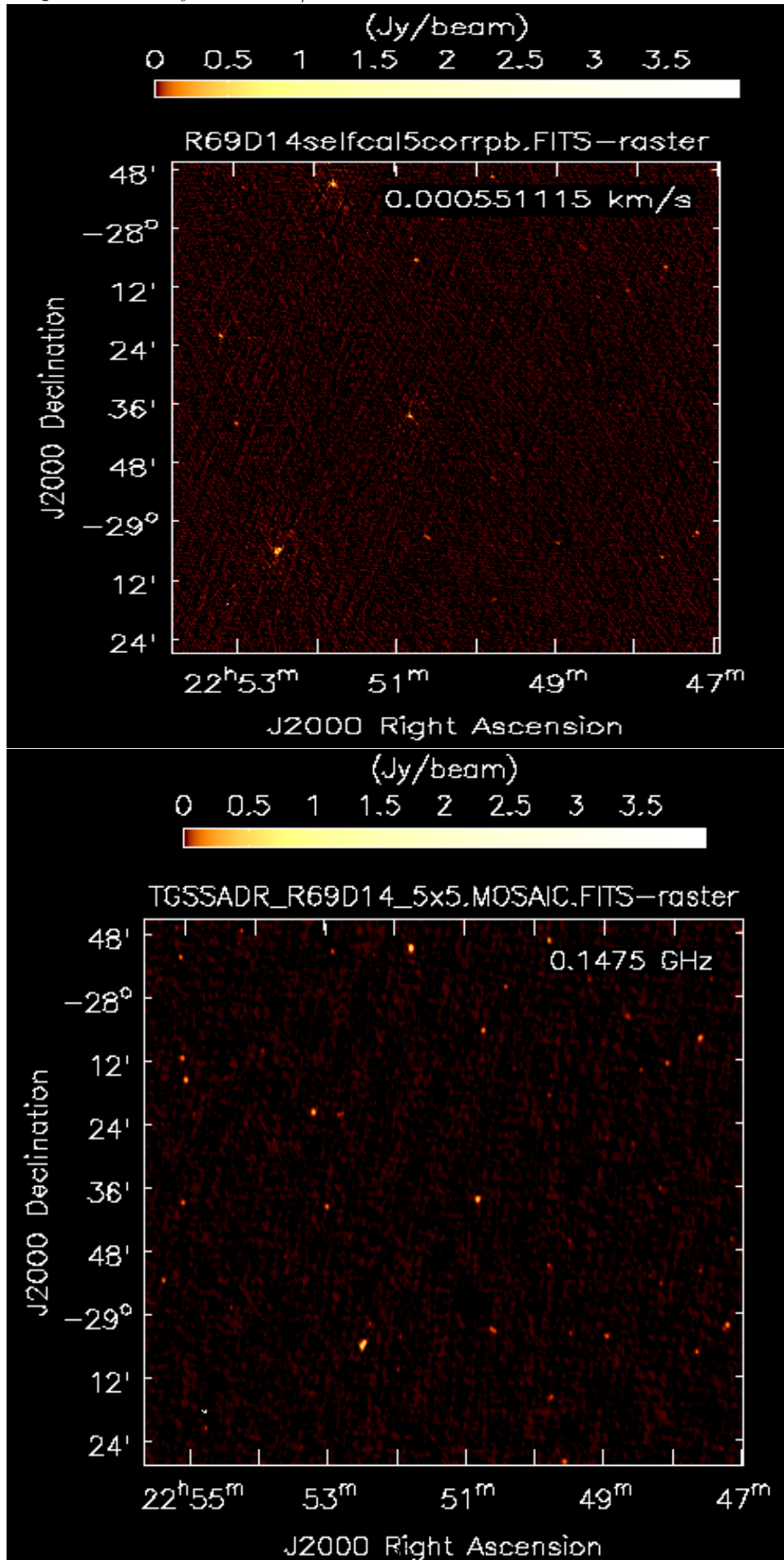


Figure 5.3: Image of Pointing R69D14 (Date of Observation: 09jul2010)

Up: Our Analysis CASA/CAPTURE Down: TGSS ADR MOSAIC

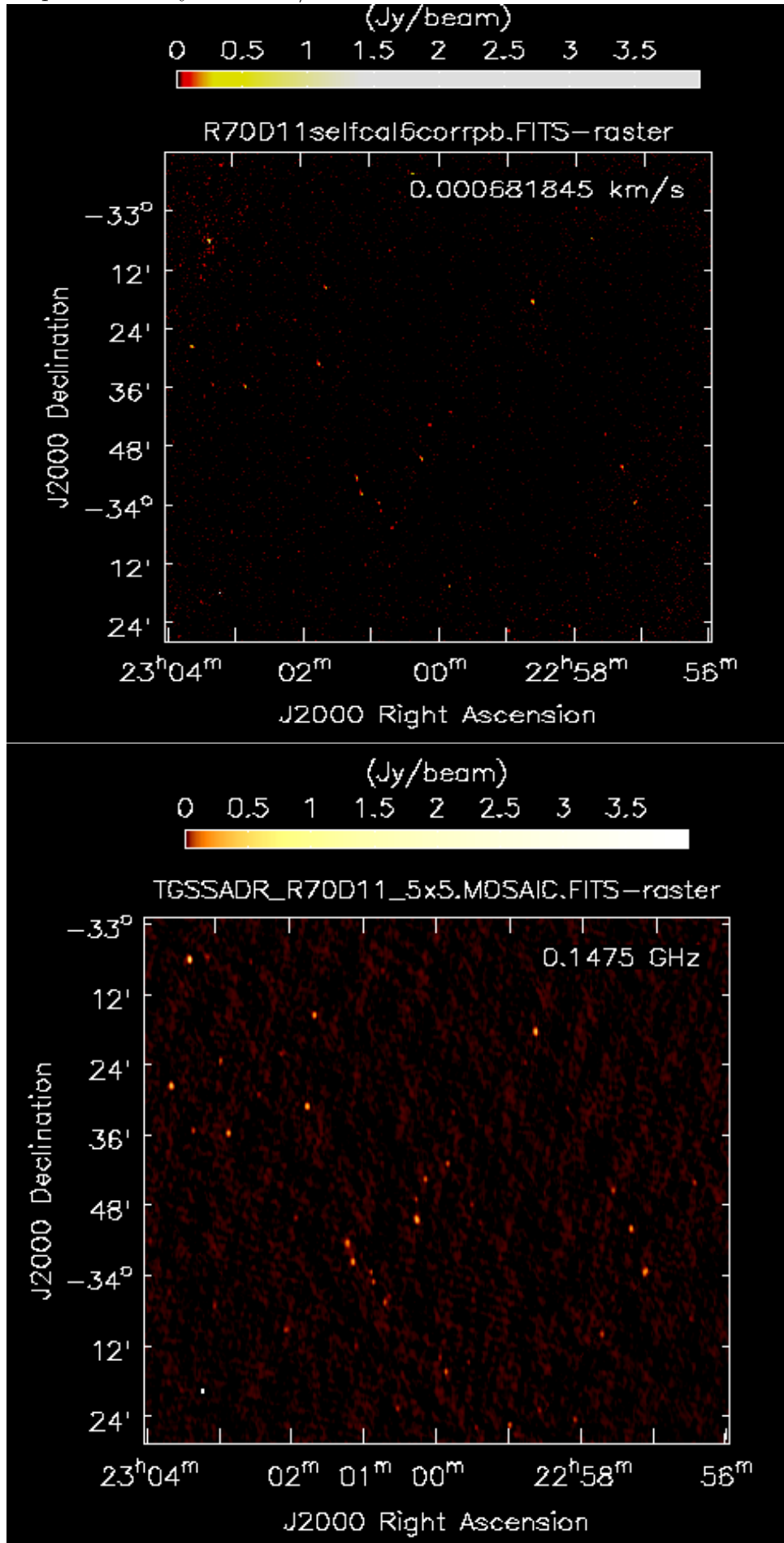


Figure 5.4: Image of Pointing R70D11 (Date of Observation: 29Aug2010)

**Quantitively** When investigating images visually one like to identify if the same sources are easily identified one to one in both the images for same pointing from our analysis and ADR mosaic and they do! Next we will like to quantitatively compare Dynamic Range given by Peak flux (Jy/beam) to RMS (Jy/beam) of signal free region. It will be great if our Dynamic range compares or even better than ADR - here we are satisfied that our Dynamic Range compares despite not having done DD calibrations. For R70D12 we are happy that our Dynamic Range is a factor of 0.9 compared to ADR.

Pointings	This Work			ADR			DR Ratio
	Peak flux (Jy/bm)	RMS (mJy/bm)	Dynamic range	Peak flux (Jy/bm)	Signal free RMS (mJy/bm)	Dynamic range	ADR/ This Work
R69D11	4.2	6.9	600	3.5	2.6	1352	2.3
R69D12	7.3	9.9	735	4.5	3.2	1413	1.9
R69D13	8.7	7.9	1106	4.7	2.6	1832	1.7
R69D14	6.6	7.4	894	4.5	3.4	1327	1.5
R70D11	5.4	8.6	627	3.3	3.5	941	1.5
R70D12	4.2	6.8	618	2.1	3.5	596	0.9
R70D13	5.5	6.9	792	4.5	3.5	1282	1.6
R70D14	4.8	7.5	649	4.4	4.8	929	1.4
R71D11	2.9	8.7	336	2.1	3.8	554	1.6

Figure 5.5: Flux, RMS & Dynamic Range Comparison between our images and ADR Mosaic

The RMS noise in signal free region is higher than in ADR - however accuracy of flux is most important. We take note that the peak fluxes of same pointings from our analysis and ADR don't match. It becomes important to understand if fluxes in our analysis is correct. For this purpose in latter section we shall use CAPTURE to get flux values for all flux and phase calibrators in TGSS and see if consistent with existing literature on other neighbouring frequencies from NASA/IPAC Extragalactic database [6].

## 5.1.2 Comparing between our work and ADR

Further we proceed to generating catalogues of sources using PyBDSF keeping default settings other than "adaptive\_rms\_box = True" and "thresh = 'hard'" for each pointing from our primary beam corrected image and available ADR 5\*5  $deg^2$  MOSAIC. Then match the sources from the 2 catalogues by RA,DEC within estimated RA,DEC error and ultimately take ratio of flux (both peak flux in Jy/beam and integrated flux in Jy) for those sources (source code 'S' in PyBDSF) which were fit by a single gaussian only. Ideally we want to compare flux of unresolved sources only and the systematic offset of mean values (ignoring the error bar!) between ratios of Peak flux Jy/beam and Integrated Flux Jy probably indicates that a few of the 'S' sources are slightly extended. This way we could check for system flux offset per pointing. But one thing to note is we have continued using primary beam coefficients as available in GMRT's observers manual while ADR team had updated the primary beam model for their work. [25]

### Flux Comparison between same unresolved (point) or slightly extended sources

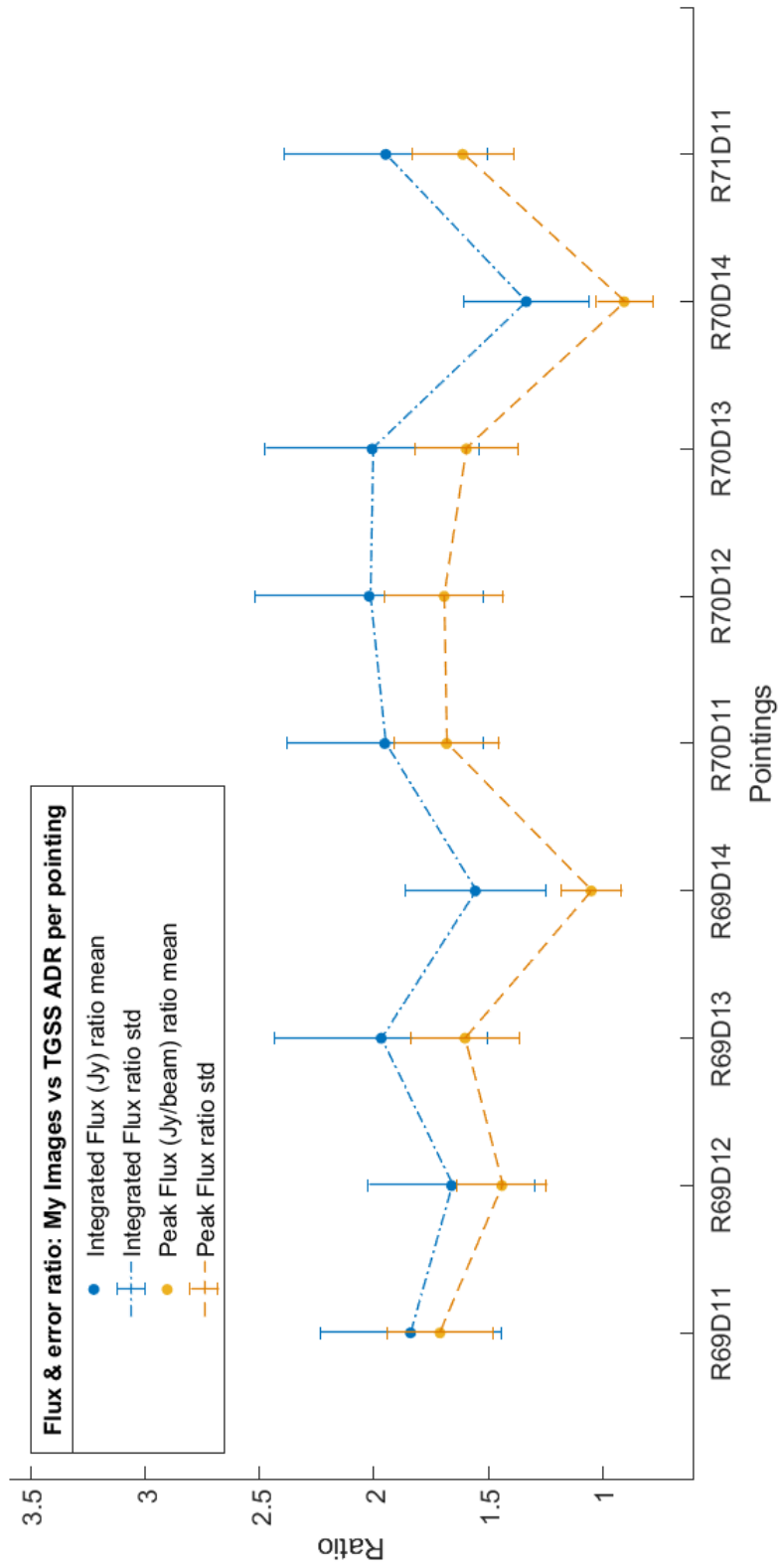
We tabulate descriptive statistics for ratio of peak flux (Jy/beam) then integrated flux (Jy) per pointing between sources matched by RA,Dec in our image and ADR MOSAIC, and finally show a plot containing 'mean' and standard deviation from both tables. The columns in table are: Pointing name, count meaning number of sources matched to arrive at its descriptive statistics, arithmetic mean, standard deviation, minimum value of ratio through percentile 25 till 75 and then maximum value.

Pointings	count	mean	std	min	25 p	50 p	75 p	max
R69D11	201	1.710+/- 0.230	0.473+/- 0.208	0.701+/- 0.011	1.438+/- 0.082	1.708+/- 0.167	1.947+/- 0.327	3.906+/- 1.284
R69D12	123	1.441+/- 0.194	0.465+/- 0.189	0.714+/- 0.012	1.151+/- 0.075	1.388+/- 0.155	1.599+/- 0.276	4.334+/- 1.503
R69D13	172	1.601+/- 0.235	0.428+/- 0.202	0.658+/- 0.013	1.346+/- 0.083	1.533+/- 0.171	1.797+/- 0.318	3.168+/- 0.945
R69D14	109	1.05+/- 0.133	0.302+/- 0.104	0.341+/- 0.012	0.832+/- 0.052	1.017+/- 0.095	1.214+/- 0.189	1.979+/- 0.512
R70D11	121	1.682+/- 0.229	0.569+/- 0.203	0.439+/- 0.015	1.300+/- 0.073	1.659+/- 0.166	2.006+/- 0.311	3.800+/- 0.934
R70D12	175	1.693+/- 0.259	0.567+/- 0.235	0.75+/- 0.018	1.358+/- 0.101	1.62+/- 0.183	1.911+/- 0.338	4.124+/- 1.264
R70D13	185	1.596+/- 0.223	0.409+/- 0.178	0.784+/- 0.02	1.318+/- 0.1	1.553+/- 0.174	1.832+/- 0.3	3.419+/- 1.095
R70D14	59	0.906+/- 0.123	0.301+/- 0.114	0.397+/- 0.019	0.696+/- 0.044	0.919+/- 0.069	1.052+/- 0.182	1.933+/- 0.558
R71D11	127	1.611+/- 0.221	0.466+/- 0.173	0.369+/- 0.014	1.336+/- 0.081	1.614+/- 0.191	1.959+/- 0.315	3.592+/- 1.108

Table 5.1: Comparing Peak Flux between us and ADR 1 per pointing.

Pointings	count	mean	std	min	25 p	50 p	75 p	max
R69D11	201	1.840+/- 0.396	0.452+/- 0.315	0.810+/- 0.032	1.538+/- 0.158	1.785+/- 0.317	2.108+/- 0.530	3.652+/- 2.154
R69D12	123	1.660+/- 0.366	0.519+/- 0.346	0.922+/- 0.030	1.356+/- 0.145	1.589+/- 0.294	1.815+/- 0.465	4.276+/- 2.716
R69D13	172	1.968+/- 0.467	0.617+/- 0.395	0.915+/- 0.061	1.589+/- 0.181	1.848+/- 0.347	2.225+/- 0.665	4.933+/- 2.39
R69D14	109	1.556+/- 0.306	0.585+/- 0.252	0.514+/- 0.038	1.203+/- 0.132	1.463+/- 0.233	1.844+/- 0.401	5.159+/- 1.535
R70D11	121	1.952+/- 0.43	0.582+/- 0.345	0.549+/- 0.055	1.607+/- 0.157	1.866+/- 0.326	2.183+/- 0.632	4.288+/- 1.803
R70D12	175	2.021+/- 0.499	0.698+/- 0.445	0.669+/- 0.046	1.583+/- 0.2	1.866+/- 0.371	2.316+/- 0.636	5.098+/- 2.278
R70D13	185	2.008+/- 0.468	0.737+/- 0.424	0.823+/- 0.044	1.649+/- 0.188	1.897+/- 0.350	2.199+/- 0.607	8.686+/- 3.290
R70D14	59	1.333+/- 0.273	0.565+/- 0.270	0.395+/- 0.033	0.95+/- 0.103	1.265+/- 0.188	1.584+/- 0.351	3.735+/- 1.723
R71D11	127	1.948+/- 0.447	0.703+/- 0.351	0.432+/- 0.05	1.556+/- 0.163	1.852+/- 0.362	2.173+/- 0.611	5.460+/- 1.506

Table 5.2: Comparing Integrated Flux between us and ADR 1 per pointing.



33  
 Figure 5.6: Ratio of Peak and Integrated Flux from our images and ADR Mosaic

## 5.2 Flux Comparison using all Flux and Phase Calibrators in TGSS

In order to understand if our fluxes are correct first we see the flux values for flux calibrators 3C48, 3C286, 3C147 from ADR MOSAIC/cutout and as per standards- Perley Taylor 1999, Scaife Heald 2012 and Perley Butler 2017 at the given frequency.

Flux Calibrators	ADR Mosaic, 147.5 MHz	Perley Taylor 1999, 156 MHz	Scaife Heald 2012, 156 MHz	Perley-Butler 2017, 156 MHz
3C48	66.97 +/- 0.16	62.891	63.78	62.369
3C286	17.34 +/- 0.03	31.055	27.309	29.92
3C147	67.84 +/- 0.19	67.964	66.637	69.623

Table 5.3: Flux calibrator values in Jy from ADR & flux models

Flux value of 3C286 from ADR comes wrong. It is interesting to note that even during ADR1 they had found that apparent flux density of 3C286 was off the trend from other primary calibrators 3C 48, 3C 147, 3C 196, 3C 295 and 3C 380 - and they think this is due to a simultaneous and persisting phase delay jumps on about 10 antennas as being the cause. Hence calibrating for delay jump will be an integral part of future ADR2 release. Also they don't believe that due to systematically low value of 3C286 in ADR1, flux scale of majority observations will be affected. [25]

### 5.2.1 Our Analysis in Standard scales vs ADR

We further see how the flux compares (in all 3 available standards at this frequency Perley Butler 2017, Perley-Taylor 99 and Scaife-Heald 2012), for 29 phase calibrators as per our analysis from downloaded raw data (over 1500 GB!) of relevant TGSS scans and measured from ADR mosaics/cutouts. The 29 phase calibrators are numbered from 1 to 29 for the plot in following order-0025-260,0116-208,0141+138,0323+055,0409-179,0432+416,0521+166, 0521-207,0744-064,0834+555,0837-198,1021+219,1033-343,1119-030,1154-350,1311-222,1419+064, 1459+716,1714-252,1822-096,1830-360,1833-210,2038+513,2047-026,2206-185,2219-279, 2225-049,2341-351 & 2350+646.

Only for 5 out of 29 phase calibrators namely 1714-252, 1822-096, 1830-360, 1833-210 & 2350+646, ADR MOSAIC/cutout seems to have wrong flux values which are quite higher than our work and other existing literature NASA/IPAC Extragalactic Database.

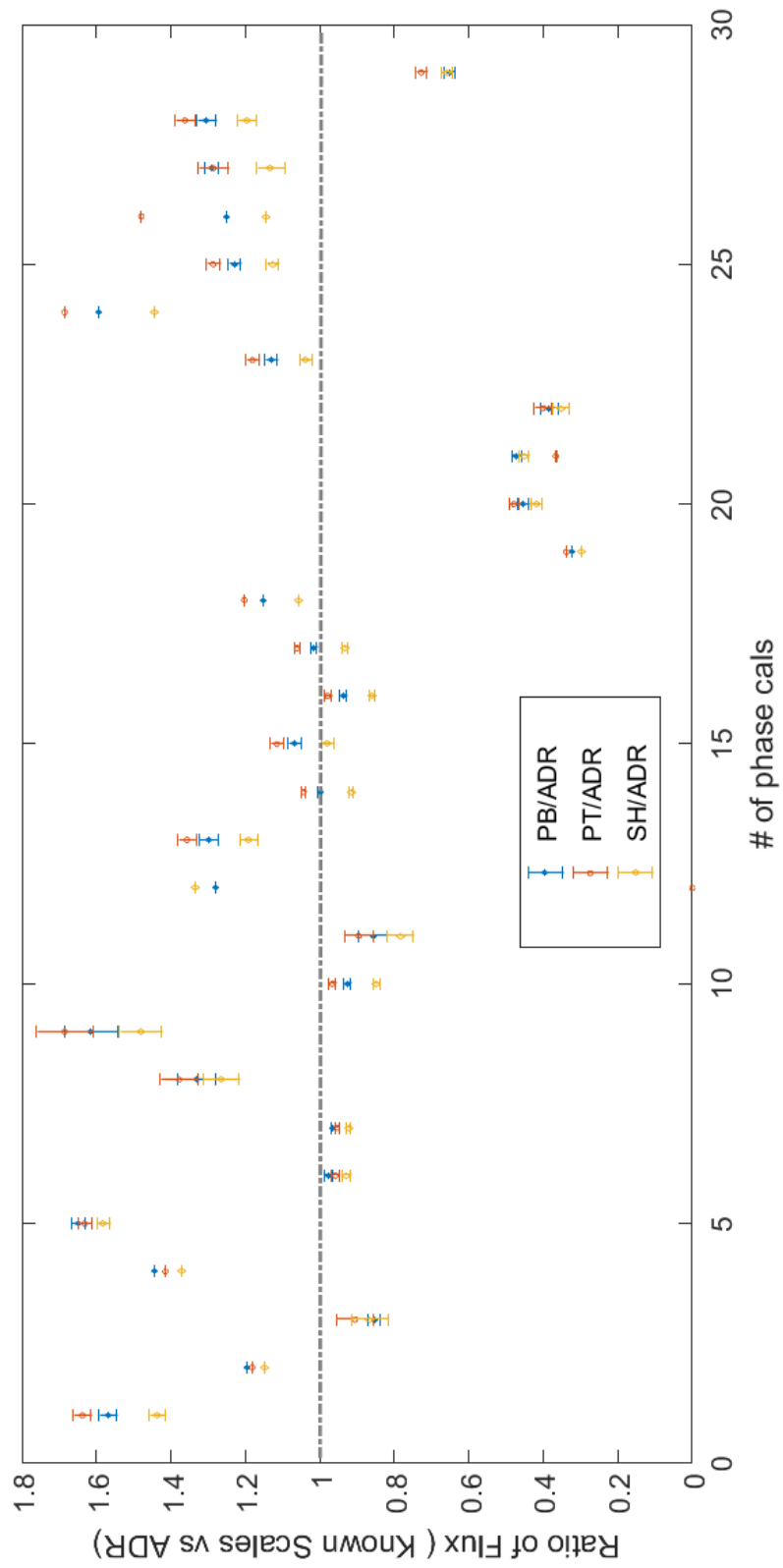


Figure 5.7: Ratio of Flux (Known Scales vs ADR) vs # of phase calcs



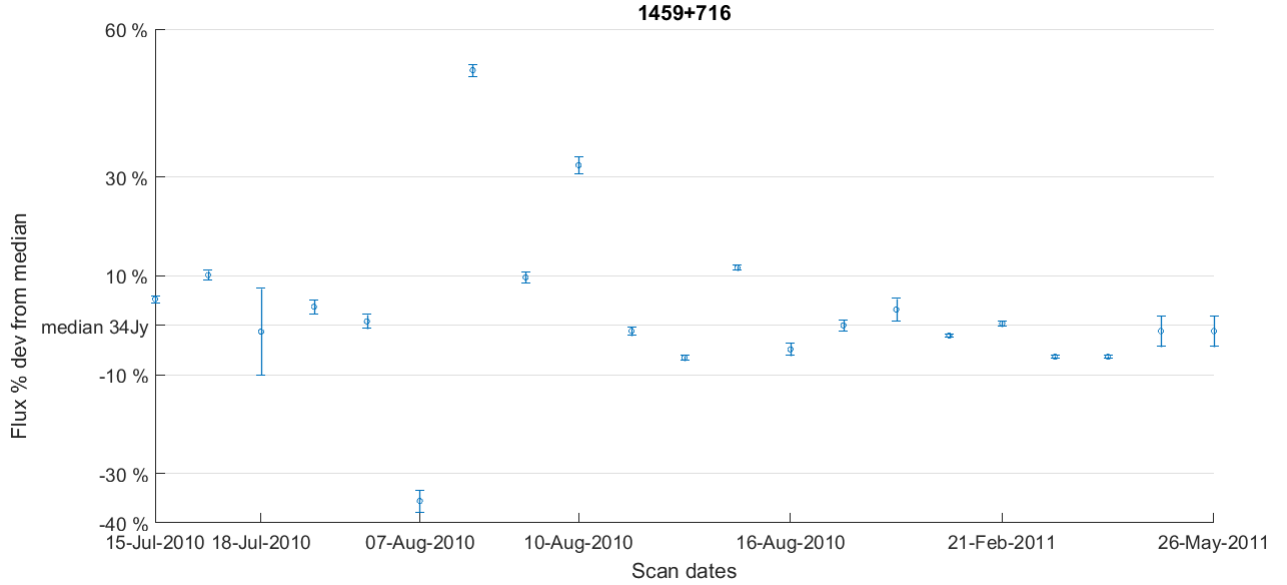


Figure 5.10: Variations of Flux in PB2017 scale per scan for 1459+716

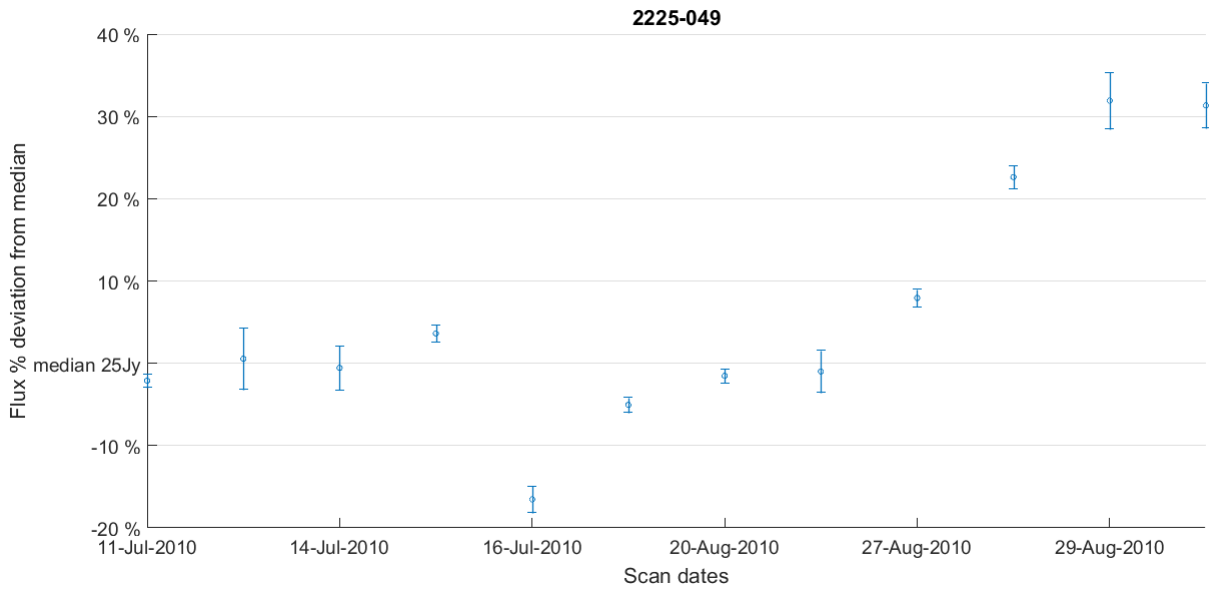


Figure 5.11: Variations of Flux in PB2017 scale per scan for 2225-049

Some outliers are easy to spot - Some scans give very high or low flux values , and it is unlikely that this should be due to a real physical process in the observed source given the variability we observe over the period don't match with what we understand about intrinsic variability of flux in some phase calibrators [18, 20]; instead the data and pipeline together may have given a wrong value.

Table 5.2 is provided with information of calculated flux value+/- error Jy as per Perley Butler 2017, SNR of phase cal uv data, number of points in uv plane N and scan identifier. We hope this helps people to be careful while using these scans in future. Also these errors

Phase Calibrator	Flux +/-err Jy	SNR	N	Scan
1311-222	0.40931 +/- 1.02963	0.397531	58	20_083_27APR2011_2S; 20_083_27APR2011
1311-222	28.1494 +/- 0.270499	104.065	58	21_057_15MAR2012
1311-222	36.3299 +/- 0.214975	168.996	52	19_043_11MAY2011
1311-222	63.0808 +/- 0.628377	100.387	60	19_043_18MAY2011
1419+064	84.0901 +/- 21.0306	3.99846	35	18_031_4MAY2010_GSB
1419+064	18.5671 +/- 1.48309	12.5192	44	18_031_18JUN10_GSB
1419+064	100.509 +/- 0.65165	154.237	56	18_031_16MAY2010_GSB
1419+064	101.008 +/- 0.446345	226.301	59	18_031_06JUL2010_GSB
1459+716	22.0049 +/- 0.759984	28.9544	48	18_031_07AUG2010
1459+716	51.8095 +/- 0.42251	122.623	57	18_031_08AUG2010
1459+716	45.239 +/- 0.592182	76.3938	53	18_031_10AUG2010
2225-049	21.013 +/- 0.40585	51.7754	57	18_031_16JUL2010
2225-049	30.8708 +/- 0.350416	88.0975	58	18_031_28AUG2010
2225-049	33.2067 +/- 0.867346	38.2854	53	18_031_29AUG2010
2225-049	33.0606 +/- 0.682911	8.4112	50	18_031_30AUG2010
0141+138	12.7087 +/- 0.0813855	156.154	60	19_043_01NOV2010
0141+138	12.6194 +/- 0.0779919	161.804	56	19_043_28OCT2010
0141+138	9.54811 +/- 0.512376	18.635	58	19_043_19OCT2010
0141+138	19.5235 +/- 1.38149	14.1322	34	19_043_30OCT2010
0141+138	13.0628 +/- 0.0602065	216.967	60	19_043_31OCT2010

Table 5.4: PB 2017 Flux values, SNR and scan details for outliers.

may provide an opportunity to improve the reliability of 'CAPTURE' pipeline as we learn through manual reduction of these data and infer what the pipeline now misses to account

for.

### 5.3 Mosaic image of the 9 pointings: also covers GAMA G23 field

Up: MOSAIC Down: same MOSAIC Zoomed onto GAMA 23

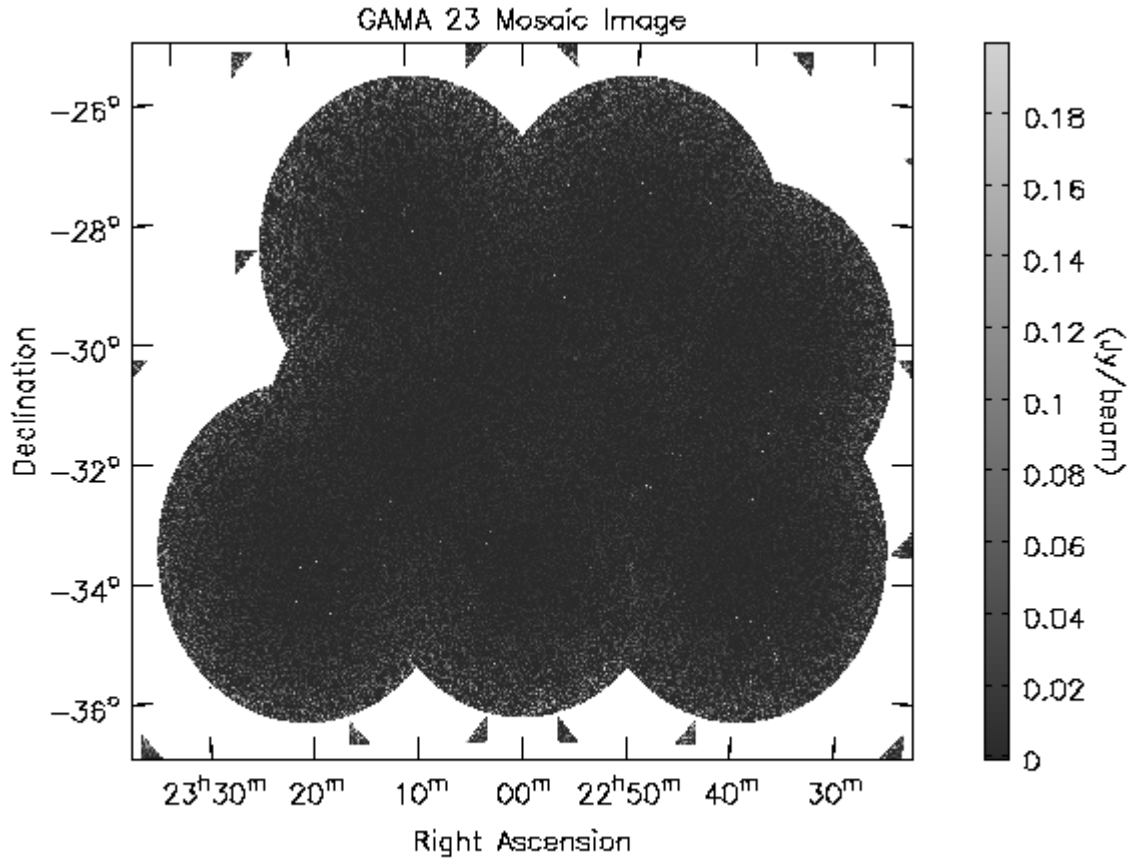


Figure 5.12: Linear mosaic of 9 pointings- R69D11 , R69D12, R69D13, R69D14, R70D11, R70D12, R70D13, R70D14 & R71D11. Mosaic center (22:59:59, -31:24:50)

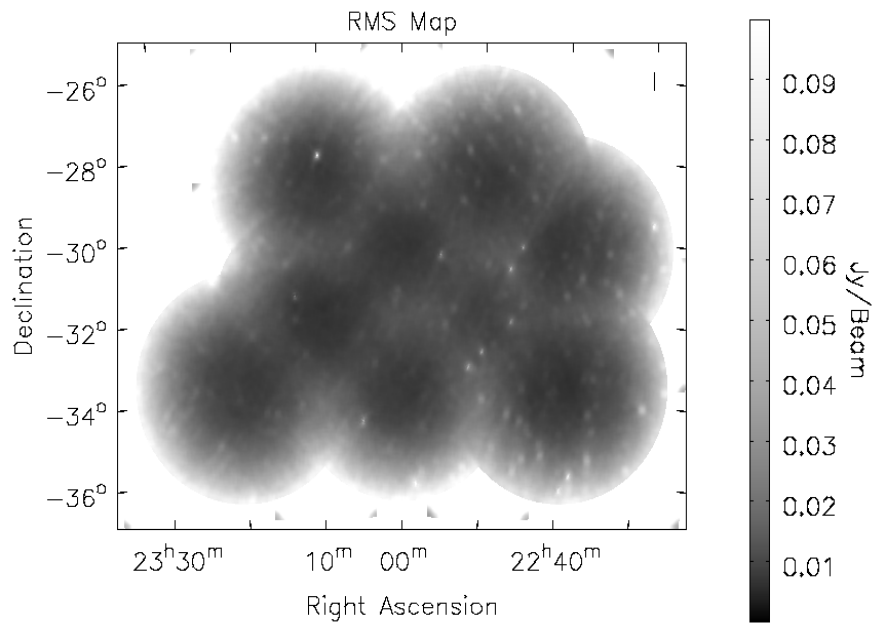


Figure 5.13: RMS Map of the MOSAIC

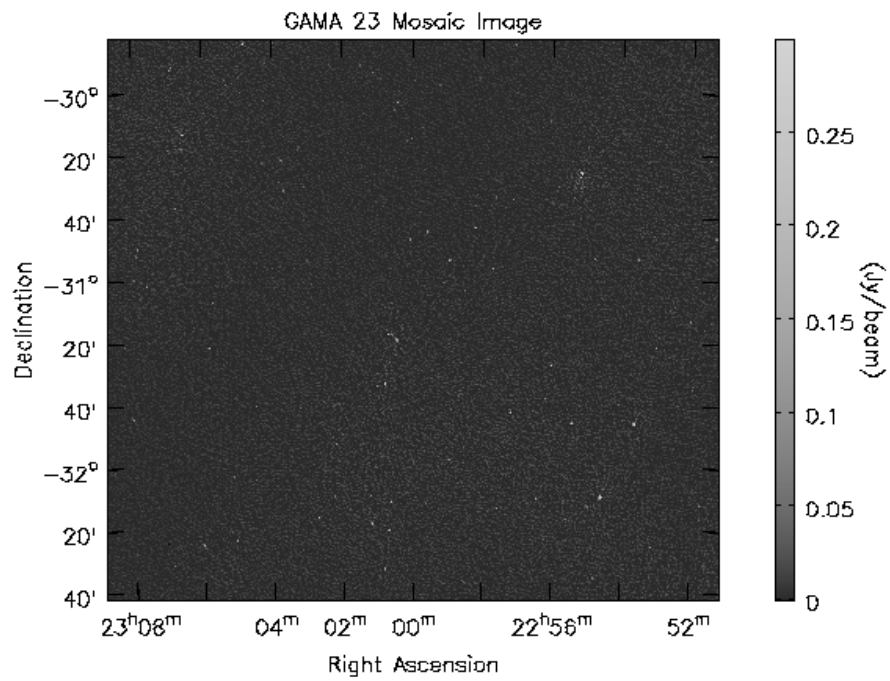


Figure 5.14: the GAMA G23 region J2000 RA (deg): 339 to 351, DEC(deg): -35 to -30

## 5.4 Source Catalog of the Mosaic Image

From the linear MOSAIC (above), using PyBDSF we generate source catalogue using non default settings like `adaptive_rms_box = True`, `psf_vary_do = True` and relevant values in `adaptive_thres`, `rms_box` and `rms_box_bright`. First we verified if the sources of flux from catalogue of MOSAIC image match with those from individual pointings within estimated flux error- we saw correct flux in 468 out of 565 matches or in 82.83 percent cases .Then we listed the integrated flux Jy for all 'S' sources and considering only fluxes above 25th percentile to max, binned them in numpy's log space. Counted the Raw number of sources in each bin N. But this raw N cannot be used without correcting each bin for [33]-

- Visibility area fraction (f): The PyBDSF RMS noise map shows how noise varies across the image. This also has an implication on the effective area per bin over which a source with a specific flux density is detectable. The Raw source count per bin is weighted down by this fraction (f). [39]
- False Detection Rate: We obtained an image with pixel values multiplied by -1 from original using 'casa.immath'. From there we extracted PyBDSF catalog and binned them exactly as we do for the original image. It is assumed that False Detection occurs due to noise spikes or bright artefacts in the image. Assuming Noise distribution is symmetric about mean, number of false detections should be equal to number of negative sources in the inverted image. Therefore fraction of real sources in each bin :

$$FDR = (N_{originalcatalog} - N_{invertedcatalog}) / (N_{originalcatalog})$$

- Completeness correction: Due to noise variation in image, all catalogs suffer from the inability to identify certain sources above flux limit. To figure the completeness fraction we start by 100 times injecting different 3000 simulated sources into PyBDSF Gaussian residual image of the original PyBDSF fitted image. 2000 of them were point/unresolved sources having size  $< 20''$  (GMRT psf at 150 MHz!) and 1000 are extended having size  $> 20''$  having random sizes uniformly distributed between the lower and upper size limit as in original extracted catalogue. The flux was also chosen to be random and uniformly lie between the original flux range as used for binning and a power law  $dN/dS \propto S^{-1.6}$  [15]. Next we extract the sources from simulated & source injected images using exact same settings in PyBDSF as used for original image. So Completeness Correction per bin  $i = 3000 / (N_{recovered,i})$

N was divided by the total mosaic image area  $\Omega$  (19.95 sq deg or 0.006 str) and bin width  $\delta S$  (upper flux limit- lower flux limit)in Jy. Central value of Flux  $S_c$  for each bin is taken as  $0.5 * (\text{upper flux limit} + \text{lower flux limit})$ . So Differential Source Count is given by  $N / (\delta S * \Omega)$  plotted against  $S_c$  while to get it Euclidean normalized  $S_c^{2.5}$ . We tabulate and show graph in the following section:

### 5.4.1 Differential Source Count (DSC)

mid mJy	S	Completeness Correction factor	raw dN/dS	raw dN/dS error	corr dN/dS	corr error	dN/dS
49.566		5.586	304.159	37.128	1699.035	207.399	
74.800		2.037	737.326	78.709	1501.933	160.329	
112.880		1.327	1122.178	132.2 09	1489.130	175.441	
170.347		1.058	1717.919	222.725	1817.558	235.643	
257.069		0.886	2136.592	338.195	1893.021	299.640	
387.943		0.779	3180.937	561.851	2477.950	437.682	
585.443		0.715	4344.616	894.040	3106.400	639.239	
883.490		0.768	4482.543	1236.464	3442.593	949.604	
1333.271		0.932	6880.173	2085.723	6412.321	1943.894	
2012.035		1.154	7689.413	3002.211	8873.582	3464.552	
3036.355		1.279	12168.944	5142.317	15564.079	6577.024	
4582.153		1.360	7090.112	5344.373	9642.552	7268.347	
6914.912		1.355	15533.856	10770.791	21048.375	14594.422	
10435.269		1.456	8860.770	11075.962	12901.280	16126.601	

Table 5.5: Table shows Differential Source Count in  $Jy^{-1}Sr^{-1}$

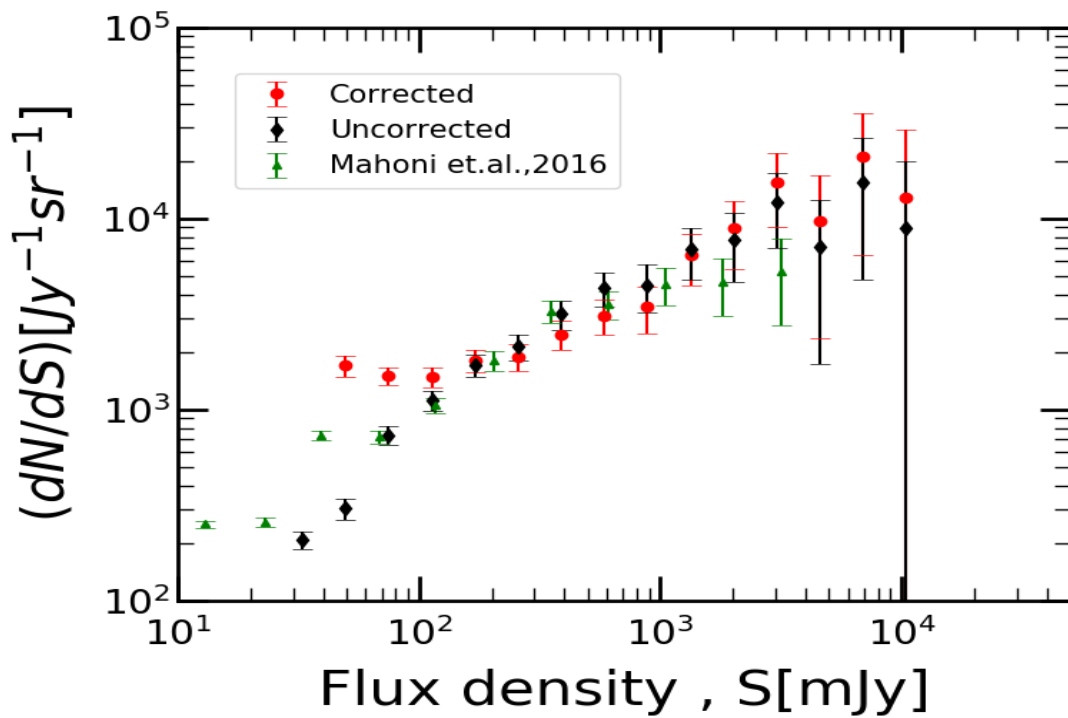


Figure 5.15: Differential source count

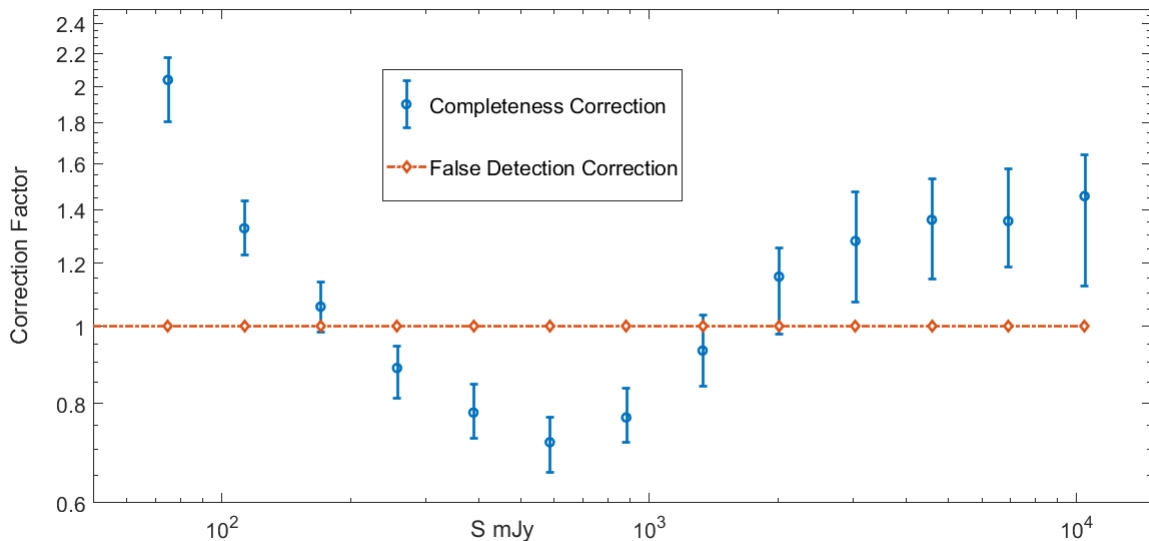


Figure 5.16: Correction factors per flux bin mJy.

At lower fluxes below 100 mJy the catalogue may not be reliable as evident from the high completeness term (and subsequently the corrected counts) implying that at these fluxes, the recovery rate is very low. This is expected since the RMS Noise in our images goes upto 10 mJy/beam hence the lower fluxes are not much significantly higher from noise RMS. Upto about 200 mJy, the counts are in reasonable agreement with Mahony et al.[32], and also the uncorrected and corrected counts are not much different.

#### 5.4.2 Matching with NVSS catalog to Spectral Indices

The NRAO's VLA Sky Survey (NVSS) [13] is an important continuum survey at 1.4 GHz covering sky north of -40 degree declination. NVSS is intended to be a service to the community and makes a catalog of over 1.8 million sources publicly available. From there, we searched the NVSS [13] for all sources within 27249.0 arcsec of 23 00 0.000 -31 13 0.00 for this covers our MOSAIC area. We also searched the VLA's FIRST survey [11] but this area is not covered. From our 9 pointings we had extracted 3632 sources, and now we could match 2043 of them in the downloaded NVSS catalog. The source were matched within a RA,DEC error threshold of 0.01 deg or 36 " judging from the max reported RA,DEC error in the downloaded NVSS catalogs and our PyBDSF catalogs.

Since Flux Density  $S \propto frequency f^{-\alpha}$  where  $\alpha$  is the spectral index, and we have flux density of 2043 sources at two frequencies 0.15 GHz (from TGSS) and 1.4 GHz (from NVSS). We can find spectral index for each source in following way-

$$\log(S_{0.15}/S_{1.4}) = -\alpha * \log(0.15/1.4). \text{ or } \alpha = \log(S_{0.15}/S_{1.4})/\log(1.4/0.15)$$

The error in spectral index due to propogation of error during division of the quantities in logarithm was found to depend only on the flux errors and flux in the following way :

$$\sqrt{(MOS : error/flux)^2 + (NVSS : error/flux)^2}$$

	<b>i</b>	<b>j</b>	<b>mosRA</b>	<b>NVRA</b>	<b>mosDec</b>	<b>NVDec</b>	<b>mosF</b>	<b>mosFe</b>	<b>NVF</b>	<b>NVFe</b>	<b>spectral index</b>	<b>err spectral index</b>
<b>0</b>	50	8897	352.980911	352.980167	-33.096829	-33.094889	649.354687	147.349111	66.6	2.1	1.019557	0.229097
<b>1</b>	51	8900	352.993229	352.991250	-34.403532	-34.402139	757.102970	175.066990	57.3	5.1	1.155627	0.247771
<b>2</b>	52	8795	352.642528	352.643667	-33.005920	-33.002750	615.279577	65.984946	77.7	2.9	0.926410	0.113553
<b>3</b>	53	8744	352.508142	352.509000	-34.187006	-34.184611	1945.770461	111.645433	36.7	7.9	1.777691	0.222775
<b>4</b>	54	8712	352.389436	352.390292	-34.545913	-34.542750	638.647254	58.810206	5.2	3.2	2.153792	0.622236
...	...	...	...	...	...	...	...	...	...	...	...	...
<b>2038</b>	3600	303	337.385000	337.383083	-32.515082	-32.517056	177.894197	49.431534	26.6	0.9	0.850772	0.279923
<b>2039</b>	3604	236	337.181153	337.180958	-32.334111	-32.334417	2207.649544	117.188051	49.5	8.5	1.700271	0.179735
<b>2040</b>	3605	131	336.812836	336.813042	-32.938799	-32.938750	866.471884	96.478944	51.8	5.4	1.261215	0.152531
<b>2041</b>	3607	102	336.716883	336.716250	-32.918497	-32.920528	1240.634835	141.745629	51.1	5.1	1.428011	0.151705
<b>2042</b>	3609	89	336.668267	336.669042	-33.605929	-33.605389	1845.742784	109.975666	5.5	3.2	2.603828	0.584861

Figure 5.17: Matching between our catalog & NVSS within RA,DEC error. This full 2043 rows  $\times$  12 columns catalog is available with author.

Histogram may be found below:

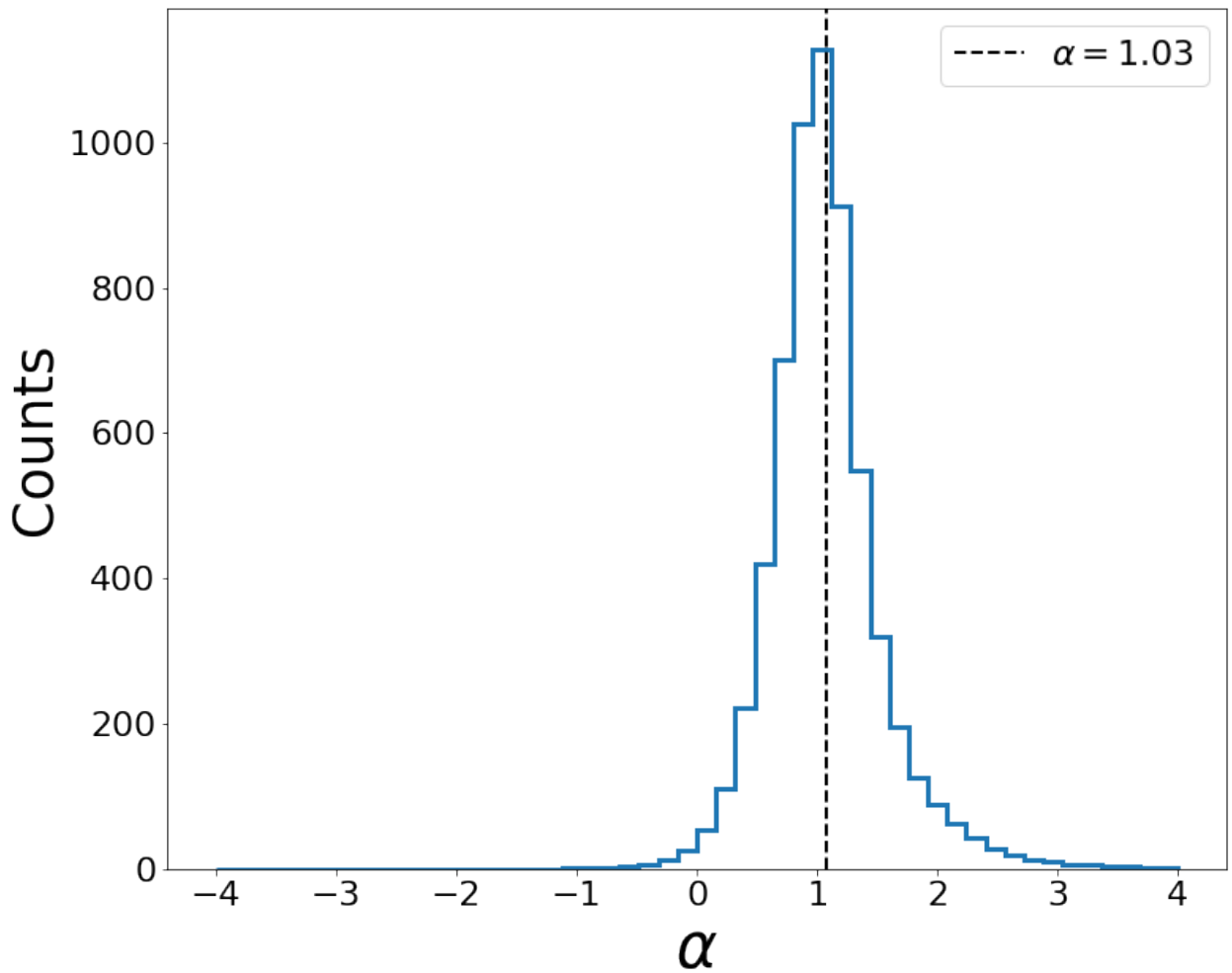


Figure 5.18: Histogram of spectral indices of matched 2043 sources.

So we got median measured combine spectral index to be 1.03 and its error 1.21. Speaking bayesian, the usually expected value of 0.8 is not ruled out but we may be seeing a natural selection bias towards a higher value of spectral index due to possible significant contribution of Radio relics at low frequencies.

# Chapter 6

## Conclusions and Scope for Future Work

Continuum surveys take place over a long amount of time, it is very important to ensure calibration went well and that the flux is accurate in every scan. This is why we obtained flux in all available three models for all TGSS Flux and phase calibrators. There are several benefits that follows from the current work apart from educational and my first hand experience in topics of radio astronomy intereferometry, data pipelines, calibration and how to do extra galactic science etc.

- First CAPTURE was untested at 150 MHz (band 2 of uGMRT). From this work people can be assured about accuracy of flux that comes out from using CAPTURE at this low frequency. Also two sample settings that works with the legacy GMRT data at 150 MHz has been found. How we arrived at the setting as documented here is equally useful as people can arrive at optimum use this way as per need. Further we show that though CAPTURE includes only upto self calibration (Direction Independent calibration) one can obtain very good quality, high dynamic range images., low RMS noise and accurate flux images.
- We gain knowledge about CAPTURE runtime errors. This should help improve CAPTURE pipeline for seem less automatic data reduction from raw data through calibrated visibilities to science ready images which otherwise consumes months of manual efforts and also the possibility of human error. Several new functionalities and improvements such as how it does delay calibration, splitting out visibilities for calibrators also if needed and concious choice of which flux standard to use etc have been added. We truly hope as use of CAPTURE pipeline for legacy GMRT or uGMRT continuum survey reduction gains popularity in public these efforts are appreciated.
- This work is first to compare flux of all calibrators (3 flux & 29 phase calibrators) in TGSS, in addition to comparing of other point sources (as extracted by PyBDSF catalog) to study systematically flux discrepancy of ADR. We indeed found atleast 5 phase calibrators namely 1714-252, 1822-096, 1830-360, 1833-210 & 2350+646 along with flux calibrator 3C286 to have incorrect fluxes in ADR. In addition fluxes in our Images of pointings is higher than ADR by a factor upto 2. This is significant because accuracy of flux at low frequency radio astronomy is critical for all radio astronomers and researchers will tend to blindly do their science using ADR

MOSAICS/cutouts eventually unidentified errors will enter unintentionally in the scientific results.

- MOSAIC of an important region of sky has been obtained from there Differential Source Count and Spectral Index was obtained as sanity check. The Differential Source Count was overlay with that from Mahony etal 2016 [32]. The spectral index and its error is also within expectation.

We shall be extremely happy to see this current work forms the basis of many future research endeavours. We can make the following wish list:

- Currently CAPTURE does not include Direction Dependant Calibration and no available CASA based pipeline does. SPAM which is AIPS based is only known to include one. People should try to make DD Facet from cubical to work with CAPTURE.
- We have obtained a statistical study of a region of sky and confirmed it to be consistent with existing literature- which is the first step, however next should be to look at the individual sources. One obvious next step is to find the optical counterparts for all 2043 radio sources for which spectral indices has been obtained.
- This work may also prepare its readers for characterizing foregrounds which when subtracted will allow to probe the weak signals from 'Epoch of Re ionization' using redshifted H 21 cm line. For example at 150 MHz, this corresponding to redshift  $z=8.5$  for H 21 cm line. Although for this they need to go deeper with perhaps other longer duration observations from GMRT such that noise is in micro Jy level.

# Bibliography

- [1] The common astronomy software application (casa) - nasa/ads <https://ui.adsabs.harvard.edu/abs/2008aspc..394..623j/abstract>.
- [2] Continuum survey - nadresearchblog [https://sites.google.com/site/nadresearchblog/home/continuum\\_survey](https://sites.google.com/site/nadresearchblog/home/continuum_survey).
- [3] Gama field locations <https://www.astro.ljmu.ac.uk/ikb/research/gamafields/>.
- [4] huibintemaspampipeline [intema] <http://www.intema.nl/doku.php?id=huibintemaspampipeline>.
- [5] Imaging - nasa/ads <https://ui.adsabs.harvard.edu/abs/1989aspc....6..117s/abstract>.
- [6] Nasa/ipac extragalactic database <https://ned.ipac.caltech.edu/>.
- [7] start [tgss adr] <http://tgssadr.strw.leidenuniv.nl/doku.php>.
- [8] A training project report on observing 21cm line with horn antenna [https://www.poornima.edu.in/wp-content/uploads/2018/pdf/24-08-2018\\_eti\\_ucaa\\_report.pdf](https://www.poornima.edu.in/wp-content/uploads/2018/pdf/24-08-2018_eti_ucaa_report.pdf).
- [9] What are radio telescopes? - national radio astronomy observatory <https://public.nrao.edu/telescopes/radio-telescopes/>.
- [10] Why is the very large array y-shaped? - national radio astronomy observatory <https://public.nrao.edu/ask/why-is-the-very-large-array-y-shaped/>.
- [11] R. H. Becker, R. L. White, and D. J. Helfand. The FIRST Survey: Faint Images of the Radio Sky at Twenty Centimeters. , 450:559, Sept. 1995.
- [12] J. J. Condon. Radio emission from normal galaxies. , 30:575–611, Jan. 1992.
- [13] J. J. Condon, W. D. Cotton, E. W. Greisen, Q. F. Yin, R. A. Perley, G. B. Taylor, and J. J. Broderick. The NRAO VLA Sky Survey. , 115(5):1693–1716, May 1998.
- [14] L. Danese, G. de Zotti, A. Franceschini, and L. Toffolatti. Interpretation of Deep Counts of Radio Sources. , 318:L15, July 1987.
- [15] F. de Gasperin, T. J. Dijkema, A. Drabent, M. Mevius, D. Rafferty, R. van Weeren, M. Brügger, J. R. Callingham, K. L. Emig, G. Heald, H. T. Intema, L. K. Morabito, A. R. Offringa, R. Oonk, E. Orrù, H. Röttgering, J. Sabater, T. Shimwell, A. Shulevski, and W. Williams. Systematic effects in LOFAR data: A unified calibration strategy. , 622:A5, Feb. 2019.

- [16] S. P. Driver, D. T. Hill, L. S. Kelvin, A. S. G. Robotham, J. Liske, P. Norberg, I. K. Baldry, S. P. Bamford, A. M. Hopkins, J. Loveday, J. A. Peacock, E. Andrae, J. Bland-Hawthorn, S. Brough, M. J. I. Brown, E. Cameron, J. H. Y. Ching, M. Colless, C. J. Conselice, S. M. Croom, N. J. G. Cross, R. D. Propris, S. Dye, M. J. Drinkwater, S. Ellis, A. W. Graham, M. W. Grootes, M. Gunawardhana, D. H. Jones, E. V. Kampen, C. Maraston, R. C. Nichol, H. R. Parkinson, S. Phillipps, K. Pimblett, C. C. Popescu, M. Prescott, I. G. Roseboom, E. M. Sadler, A. E. Sansom, R. G. Sharp, D. J. B. Smith, E. Taylor, D. Thomas, R. J. Tuffs, D. Wijesinghe, L. Dunne, C. S. Frenk, M. J. Jarvis, B. F. Madore, M. J. Meyer, M. Seibert, L. Staveley-Smith, W. J. Sutherland, and S. J. Warren. Galaxy and mass assembly (gama): survey diagnostics and core data release, 2010.
- [17] S. P. Driver, P. Norberg, I. K. Baldry, S. P. Bamford, A. M. Hopkins, J. Liske, J. Loveday, J. A. Peacock, D. T. Hill, L. S. Kelvin, A. S. G. Robotham, N. J. Cross, H. R. Parkinson, M. Prescott, C. J. Conselice, L. Dunne, S. Brough, H. Jones, R. G. Sharp, E. van Kampen, S. Oliver, I. G. Roseboom, J. Bland-Hawthorn, S. M. Croom, S. Ellis, E. Cameron, S. Cole, C. S. Frenk, W. J. Couch, A. W. Graham, R. Proctor, R. D. Propris, I. F. Doyle, E. M. Edmondson, R. C. N. D. Thomas, S. A. Eales, M. J. Jarvis, K. Kuijken, O. Lahav, B. F. Madore, M. Seibert, M. J. Meyer, L. Staveley-Smith, S. Phillipps, C. C. Popescu, A. E. Sansom, W. J. Sutherland, R. J. Tuffs, and S. J. Warren. Gama: towards a physical understanding of galaxy formation. *Astronomy and Geophysics*, 50:5.12–5.19, 10 2009.
- [18] C. Fanti, R. Fanti, A. Ficarra, L. Gregorini, F. Mantovani, and L. Padrielli. The low frequency variability of extragalactic radio sources : discussion of the properties. , 118:171–179, Feb. 1983.
- [19] E. B. Fomalont, K. I. Kellermann, J. V. Wall, and D. Weistrop. A Deep 6-Centimeter Radio Source Survey. *Science*, 225(4657):23–28, July 1984.
- [20] B. M. Gaensler and R. W. Hunstead. Long-term Monitoring of Molonglo Calibrators. , 17(1):72–82, Apr. 2000.
- [21] Y. Gupta, B. Ajithkumar, H. S. Kale, S. Nayak, S. Sabhapathy, S. Sureshkumar, R. V. Swami, J. N. Chengalur, S. K. Ghosh, C. H. Ishwara-Chandra, B. C. Joshi, N. Kanekar, D. V. Lal, and S. Roy. The upgraded gmrt: opening new windows on the radio universe, 2017.
- [22] D. B. Haarsma, R. B. Partridge, R. A. Windhorst, and E. A. Richards. Faint Radio Sources and Star Formation History. , 544(2):641–658, Dec. 2000.
- [23] B. Henkel and R. B. Partridge. Completing the Counts of Radio Sources at 8.5 GHz. , 635(2):950–958, Dec. 2005.
- [24] H. T. Intema. Spam: A data reduction recipe for high-resolution, low-frequency radio-interferometric observations, 2014.
- [25] H. T. Intema, P. Jagannathan, K. P. Mooley, and D. A. Frail. The gmrt 150 mhz all-sky radio survey first alternative data release tgss adr1, 2016.
- [26] C. H. Ishwara-Chandra, S. K. Sirothia, Y. Wadadekar, S. Pal, and R. Windhorst. Deep gmrt 150 mhz observations of the lbd-lynx region: Ultra-steep spectrum radio sources, 2009.

- [27] C. A. Jackson and J. V. Wall. Extragalactic radio-source evolution under the dual-population unification scheme. , 304(1):160–174, Mar. 1999.
- [28] D. L. Jauncey. Radio surveys and source counts. , 13:23–44, Jan. 1975.
- [29] R. Kale and I.-C. C. H. Capture: A continuum imaging pipeline for the ugmrt. 10 2020.
- [30] A. Kepley and C. Brogan. When, why, and how to do self-calibration sabrina stierwalt.
- [31] D. A. Leahy, A. Hopkins, R. P. Norris, J. Marvil, J. Collier, E. Taylor, J. Allison, C. Anderson, M. Bell, M. Bilicki, J. Bland-Hawthorn, S. Brough, M. Brown, S. Driver, G. Gurkan, L. Harvey-Smith, I. Heywood, B. Holwerda, J. Liske, A. R. Lopez-Sanchez, D. McConnell, A. Moffett, M. Owers, K. Pimblet, W. Raja, N. Seymour, M. Voronkov, and L. Wang. Askap commissioning observations of the gama 23 field. *Publications of the Astronomical Society of Australia*, 2019.
- [32] E. Mahony, R. Morganti, I. Prandoni, I. Bemmell, T. Shimwell, M. Brienza, P. Best, M. Brügger, G. Rivera, F. Gasperin, M. Hardcastle, J. Harwood, G. Heald, M. Jarvis, S. Mandal, G. Miley, E. Retana-Montenegro, H. Röttgering, J. Sabater, and G. White. The lockman hole project: Lofar observations and spectral index properties of low-frequency radio sources. *Monthly Notices of the Royal Astronomical Society*, 463, 09 2016.
- [33] A. Mazumder, A. Chakraborty, A. Datta, S. Choudhuri, N. Roy, Y. Wadadekar, and C. Ishwara-Chandra. Characterizing eor foregrounds: A study of the lockman hole region at 325 mhz. 05 2020.
- [34] A. D. Nska, M. J. Hardcastle, C. A. Jackson, T. An, W. A. Baan, and M. J. Jarvis. Unravelling lifecycles physics of radio-loud agn in the ska era. volume 9-13-June-2014. Proceedings of Science (PoS), 2014.
- [35] M. Ryle. The Counts of Radio Sources. , 6:249, Jan. 1968.
- [36] A. S. Hi 21cm observations of barred spiral galaxies and studies on a supernova remnant dissertation, 5 2019.
- [37] T. Shanks, V. Belokurov, B. Chehade, S. M. Croom, J. R. Findlay, E. Gonzalez-Solares, M. J. Irwin, S. Koposov, R. G. Mann, N. Metcalfe, D. N. A. Murphy, P. R. Norberg, M. A. Read, E. Sutorius, and G. Worsack. Vst atlas first science results, 2013.
- [38] R. A. Windhorst. The microJansky and nanoJansky population. , 47(4-5):357–365, Sept. 2003.
- [39] R. A. Windhorst, G. K. Miley, F. N. Owen, R. G. Kron, and D. C. Koo. Sub-millijansky 1.4 GHz source counts and multicolor studies of weak rado galaxy populations. , 289:494–513, Feb. 1985.